Article:
Barrett, BJ, Collier, RELL, Hodgson, DM et al. (2019) Quantifying faulting and base level controls on syn-rift sedimentation using stratigraphic architectures of coeval, adjacent Early-Middle Pleistocene fan deltas in Lake Corinth, Greece. Basin Research, 31 (6). pp. 1040-1065. ISSN: 0950-091X

https://doi.org/10.1111/bre.12356

Title:

Quantifying faulting and base level controls on syn-rift sedimentation using stratigraphic architectures of coeval, adjacent Early-Middle Pleistocene fan deltas in Lake Corinth, Greece

Authors: Barrett, B.J.[1], Collier, R.E.Ll.[1], Hodgson, D.M.[1], Gawthorpe, R.L.[2], Dorrell, R.M.[3] & Cullen, T[1].

[1] School of Earth & Environment, University of Leeds, Leeds, LS2 9JT, UK.

[2] Department of Earth Science, University of Bergen, Bergen, N5020, Norway.

[3] Energy and Environment Institute, University of Hull, Hull, HU6 7RX, UK.

ABSTRACT

Quantification of allogenic controls in rift basin-fills requires analysis of multiple depositional systems because of marked along-strike changes in depositional architecture. Here, we compare two coeval Early-Middle Pleistocene syn-rift fan deltas that sit 6 km apart in the hangingwall of the Pirgaki-Mamoussia Fault, along the southern margin of the Gulf of Corinth, Greece. The Selinous fan delta is located near the fault tip, and the Kerinitis fan delta towards the fault centre, but Selinous and Kerinitis have comparable overall aggradational stacking patterns. Selinous comprises fifteen cyclic stratal units (~25 m thick), whereas at Kerinitis eleven (~60 m thick) are present. Eight facies associations are identified. Fluvial and shallow water, conglomeratic facies dominate the major stratal units in the topset region, with shelfal fine-grained facies constituting ~2 m thick intervals between major topsets units, and thick conglomeratic foresets building down-dip. It is possible to quantify delta build times (Selinous: 615 kyrs; Kerinitis: >450 kyrs), and average subsidence and equivalent sedimentation rates (Selinous: 0.65 m/kyrs; Kerinitis: >1.77 m/kyrs). The presence of sequence boundaries at Selinous, but their absence at Kerinitis, enables sensitivity analysis of the most uncertain variables using a numerical model, 'Syn-Strat', supported by an independent unit thickness extrapolation method. Our study has three broad outcomes: 1) the first estimate of lake level change amplitude in Lake Corinth for the Early-Middle Pleistocene (10-15 m), which can aid regional palaeoclimate studies and inform broader climate-system models; 2) demonstration of two complementary methods to quantify faulting and base level signals in the stratigraphic record – forward modelling with Syn-Strat and a unit thickness extrapolation - which can be applied to other rift basin-fills; and 3) a

quantitative approach to the analysis of stacking patterns and key surfaces that could be applied to stratigraphic pinch-out assessment and cross-hole correlations in reservoir analysis.

1. INTRODUCTION

Distinguishing faulting, sediment supply and base level signals and quantifying these basin controls in an active rift setting remains problematic, particularly due to along-strike variability in depositional architecture. Characterisation of multiple coeval depositional systems within the same rift basin is required to resolve the record of each control. Syn-rift, Gilbert-type fan deltas (Gilbert, 1885, 1890) provide an ideal record of stratigraphic evolution to achieve this due to their position adjacent to normal growth faults, with high and variable sediment supply rates derived from independent drainage catchments. However, most previous studies focus on single systems, rather than multiple, along-strike spatially distributed deltas (e.g. Garcia-Mondéjar, 1990; Dart et al., 1994; Dorsey et al., 1995; Mortimer et al., 2005; Garcia-Garcia et al., 2006; Ford et al., 2007; Backert et al., 2010).

Previous work on the stratigraphic record around normal faults at rifted margins has focussed on the theoretical aspects of sequence development from the interplay of controls in these areas. Leeder & Gawthorpe (1987) assessed the influence of tectonically-induced slopes on facies models. Variation in stacking patterns and sequence stratigraphic surfaces across rift settings (Gawthorpe et al., 1994), and as a result of propagating normal faults (Gawthorpe et al., 1997) became the later focus. An influential series of conceptual models for tectono-sedimentary evolution in extensional basins was presented by Gawthorpe & Leeder (2000). Eustasy/base level, tectonics and sedimentation influence the nature of sedimentary stacking through the accommodation/supply ratio (Jervey, 1988; Neal & Abreu, 2009) as eustasy and tectonic subsidence act to control space available for deposition (A) and sedimentation fills that space (S). Numerical modelling has supported understanding of rift basin sequence stratigraphy, particularly as simplified tectonic constraints were introduced into forward models (Jervey et al., 1988; Hardy et al., 1994; Hardy & Gawthorpe, 1998; 2002; Ritchie et al., 1999) and stratigraphic surfaces were shown to be limited in spatial extent (Gawthorpe et al., 2003; Jackson et al., 2005). Barrett et al. (2018) demonstrate and quantify the three-dimensional and along-strike variability in sequence architecture, and diachroneity of stratigraphic surfaces in hangingwall fault blocks, using sensitivity tests with a 3D sequence stratigraphic forward model, 'Syn-Strat'. Complementary field studies have shown that sequence boundary development is best expressed at fault tip regions (Dorsey & Umhoefer, 2000 – Loreto Basin), and observed stratigraphic cyclicity has been attributed to fault-related subsidence events (Dorsey et al., 1995 – Loreto Basin) and climatic forcing (Dart et al., 1994;

Backert et al., 2010 – Gulf of Corinth). Marked differences occur in the sequence stratigraphy of two coeval fan deltas 50 km apart, due to contrasting tectonic controls between footwall (Kryoneri) and hangingwall (Kerinitis) sites (Gawthorpe et al., 2017a). However, along-strike and down-dip variation on smaller length-scales (<10 km) within the same hangingwall basin has not yet been attempted. Furthermore, quantification of tectonism, base level and sedimentation signals is also lacking. This is because isolating these controls is difficult, yet is critical to improving our understanding of palaeoenvironmental evolution and for making predictions beyond data limits.

Here, we present an integrated field and numerical modelling investigation of two adjacent and contemporaneous syn-rift fan deltas, six km along-strike from one another in the hangingwall of the same normal fault; the Pyrgaki-Mamoussia Fault. The fan deltas are referred to as the Selinous near the fault tip, and the Kerinitis near the fault centre (Fig. 1). This is the first detailed sedimentological and stratigraphic study of the Selinous fan delta, and with comparison to the Kerinitis fan delta, allows a unique insight into the controlling parameters during rift basin evolution. The aim of the study is to resolve and quantify the contribution of tectonics and base level change to sequence architecture in Lake Corinth through the Early-Middle Pleistocene. In doing so, methodologies that are applicable to any basin with given data constraints are demonstrated. To satisfy the aim, the objectives are: 1) to derive quantified estimates of the controlling parameters based on comparisons of facies, stacking patterns and the nature of key stratigraphic surfaces between the deltas, 2) to reduce uncertainty of the quantified allogenic control estimates by use of sensitivity tests with the 3D sequence stratigraphic forward model 'Syn-Strat' (Barrett et al., 2018) and to elucidate the amplitude of lake level change for Early-Middle Pleistocene Lake Corinth, 3) to validate derivations using an independent unit thickness extrapolation method; and 4) to make quantitative predictions of unit thickness along-strike variation and diachroneity of key stratigraphic surfaces. This work can be applied to other basin-fills by demonstrating two complementary methodologies for discerning and quantifying faulting and base level signals in the stratigraphic record. We undertake a quantitative analysis of unit thicknesses and surfaces that could be used in stratigraphic pinchout assessment and cross-hole correlations in syn-rift reservoirs. Finally, the palaeoclimatic data on lake level changes derived from the geological record can be used to inform climate-system models for the Pleistocene.

2. TECTONO-STRATIGRAPHIC FRAMEWORK

The Gulf of Corinth marks the axis of the ~100 km long, 60-80 km wide Corinth Rift that was activated during the Late Miocene/Early Pliocene (~5 Ma; Collier & Dart, 1991; Leeder et al., 2008; Ford et al., 2016; Gawthorpe et al., 2017b). Present-day N-S geodetic extension rates are up to 15 mm/yr (Clarke et al., 1997; Briole et al., 2000; Avallone et al., 2004; Floyd et al., 2010), which are accommodated on N- and S-dipping normal faults (McNeill et al., 2005; Bernard et al., 2006; Bell et al., 2008). The oldest part of the rift (Rift 1, ~5-3.6 to 2.2-1.8 Ma; Ford et al., 2013; 2016; Nixon et al., 2016; Gawthorpe et al., 2017b) lies furthest south in northern Peloponnesos, where faulting was focussed at that time on the Kalavryta, Doumena, Valimi Faults (Fig. 1) and other southern border faults. At this time the Kalavryta alluvial system fed sediment northwards, and fluvial and marginal lacustrine environments prevailed (Lower Group; Ford et al., 2016). In the eastern part of the rift (Fig. 1), the Kyllini, Mavro, Kefalari and Nemea fan deltas built out into the basin (as described by Gawthorpe et al., 2017b). There was an upward deepening through the 'Rift 1' sequence at ~3.6 Ma (Gawthorpe et al., 2017b) from deposition of the fluvial-marginal Korfiotissa and Ano Pitsa Formations, to the deep lacustrine Pellini and Rethi-Dendro Formations, referred to as the 'Great Deepening' (Leeder et al., 2012).

Northward migration of faulting (Goldsworthy & Jackson, 2001; Ford et al., 2013; 2016; Nixon et al., 2016) onto the Pyrgaki-Mamoussia (P-M) Fault in the west and faults to the east occurred at ~1.8 Ma (Ford et al., 2016; Gawthorpe et al., 2017b). In the immediate hangingwall of the faults, thick syn-rift fan deltas built northwards. Four syn-rift fan deltas that sit along-strike from one another in the hangingwall of the P-M Fault developed in the west: the Selinous, Kerinitis, Vouraikos and Platanos fan deltas (from W-to-E, Fig. 1). The early development of syn-rift fan deltas along the whole length of the P-M Fault suggests that it grew rapidly in length. The contemporaneous P-M Fault hangingwall fan deltas sit within the Middle Group (Ford et al., 2007; Rohais et al., 2007; Backert et al., 2010). Pollen analysis at Vouraikos was used to date the Middle Group, which constrained the development of the P-M fan deltas to the Early-Middle Pleistocene (~1.8-0.7 Ma) but within a period of 500-800 kyr (Ford et al., 2007). Subsequent northward fault migration onto the Helike fault system at ~800 ka (Ford et al., 2016) resulted in the uplift of western Plio-Pleistocene syn-rift stratigraphy in the footwall of the modern, parallel West Helike Fault, exposing a ~6 km wide fault block

terrace. During uplift, the fan deltas were subject to erosion from their own feeder rivers that now supply the modern fan delta systems on the coast.

Predominant lacustrine conditions with discrete periods of marine incursion lasted until ~600 ka, before marine conditions prevailed due to opening at the western end of the gulf to the Ionian Sea (Rion Straits) and/or at the eastern end to the Aegean Sea (Corinth Isthmus) (Collier & Thompson, 1991; Ford et al., 2016; Nixon et al., 2016; Gawthorpe et al., 2017b).

Here, we focus on the system in the hangingwall of the P-M Fault (Fig. 1), which dips 50-55° towards the north, and has a maximum throw of >1200 m. The P-M Fault strikes WNW-ESE and is traced ~24 km from SW of Aigio to SW of Akrata. The fault juxtaposes pre-rift Mesozoic limestones in the footwall against Plio-Pleistocene hangingwall syn-rift fan delta deposits. We study two syn-rift fan deltas, the Selinous that sits towards the western fault tip, and the adjacent Kerinitis that sits nearer the fault centre. The fan deltas were influenced by: a) high slip rates on the P-M Fault as a result of rapid extension across the rift; and b) cyclic lake level and sedimentation changes from climatic variations.

3. THE GILBERT-TYPE FAN DELTAS

3.1. The Kerinitis fan delta

The Kerinitis Gilbert-type fan delta is presented in Fig. 2 in the form of a 3D outcrop model and a schematic dip section from Backert et al. (2010). Kerinitis, studied since the 1990s (Ori et al., 1991; Dart et al., 1994; Gawthorpe et al., 1994; Backert et al., 2010), is exposed on the western side of the modern Kerinitis river valley (~200 m above sea level) along a 3.8 km SW-NE dip section from the P-M Fault towards the West Helike Fault. Topsets are back-tilted by ~18° and thicken towards the P-M Fault (Fig. 2). The exposed section cuts the fan delta's eastern side, where foresets dip ~25° towards N040°. The fan delta extends laterally ~6 km along the P-M Fault, west of the Kerinitis River where it interfingers with the Selinous fan delta between the village of Pyrgaki and the Taxiarches Monastery (Fig. 1). In total, Kerinitis covers an area of 15 km^2 and is ~800 m thick; the base of the fan delta is not exposed in the Kerinitis valley, but is exposed in the footwall of the West Helike Fault. The point source of the Kerinitis fan delta incised the P-M footwall at a topographic low on an early relay zone (Backert et al., 2010), shown as a hard link on the fault (Fig. 1). Its position was locked into the landscape as fault linkage occurred. We interpret the lack of deformation penetrating the

Kerinitis delta from the western end of the Mamoussia Fault to indicate early fault linkage with the Pyrgaki Fault with respect to the exposed fan delta strata.

Backert et al. (2010) undertook the most recent and comprehensive study of the Kerinitis fan delta, whereby they characterised its architecture and facies, presented a trajectory analysis, and interpreted three stages of fan delta growth linked to initiation, growth and death of the controlling P-M Fault. The fan delta is divided into three zones from south to north, comprising fan delta topsets, a transition zone, and fan delta foresets, respectively (Fig. 2). They identify four facies associations (topset, foreset, bottomset and prodelta) and 11 key surfaces. Trajectory analysis reveals abrupt landward shifts in the topset-foreset breakpoint at each key surface, followed by gradual basinward progradation through each stratal unit. The cyclic stratal units within the fan delta are interpreted to record eustatic variations upon a background subsidence-dominated regime, in which high rates of fault subsidence overcame base level falls, in agreement with earlier studies (Dart et al., 1994; Gawthorpe et al., 1994).

3.2. The Selinous fan delta

The Selinous Gilbert-type fan delta is presented in Fig. 3 using a 3D outcrop model and schematic dip section. It is referred to as Selinous in Ford et al. (2007; 2013) and Backert et al. (2010), and as Palaeo-Meganitis in Ford et al. (2016). The Selinous fan delta has a width of ~6 km and its centre sits ~4 km from the western tip of the P-M Fault. It is exposed on the western side of the modern Selinous river valley (~150 m above sea level in the valley floor) along a 6 km long SSW-NNE dip section from the P-M Fault towards the West Helike Fault. Topsets thicken and are back-tilted by ~12° towards the P-M Fault (Fig. 3). The main section is along the west side of the Selinous river valley, where foresets dip ~21° towards N310°. On the eastern side of the valley, foresets dip ~23° towards 097° (Fig. 1). The fan delta's eastern limit interfingers with foresets of Kerinitis. The base of the fan delta is exposed in the valley in the footwall of a secondary normal fault that trends parallel to the P-M Fault. The maximum thickness of Selinous is ~400 m. The point source of the Selinous fan delta incises the P-M Fault and continues to feed the Late Pleistocene and modern fan deltas. As with Kerinitis, the Selinous fan delta can also be divided into three broad zones from south to north, with the most southerly ~2 km zone comprising delta topsets, a ~1 km transition zone in the central part and a ~3 km zone of foresets and bottomsets to the north (Fig. 3).

193

194 ## 4. METHODOLOGY

195 In this study we integrate field data with numerical techniques through the five stages of
196 analysis listed below.
197 1) Facies and stratigraphic architecture are analysed in the field and augmented with
198 Unmanned Aerial Vehicle (UAV) photogrammetry-based 3D outcrop models.
199 2) Field observations and trajectory analysis of the middle-upper units of the two fan deltas
200 are used to resolve and quantify each allogenic control acting on the delta evolution.
201 3) Each control parameter (e.g. subsidence rate, sedimentation rate etc.) is assigned a
202 qualitative uncertainty value from 1-5, whereby 1 represents a very low uncertainty estimate
203 and 5 represents a very high uncertainty estimate. This is undertaken in order to ascertain
204 which variable is most uncertain and in need of refinement with numerical model testing.
205 4) The interpreted control parameters are input into 3D sequence stratigraphic forward
206 model, Syn-Strat (Barrett et al., 2018), to test the least certain parameter(s).
207 5) Finally, an independent unit thickness extrapolation technique is adopted to validate the
208 outputs of the numerical modelling.

209 ### 4.1. Facies analysis

210 The facies analysis of major stratal units and key stratigraphic surfaces was undertaken by
211 sedimentary logging at cm-scale, documenting lithology, grain size, sedimentary structures
212 and the nature of contacts. For characterising the thicker conglomeratic units, sections were
213 logged at a dm-scale with support of sketches to capture the geometry of larger-scale
214 features. Palaeocurrent data were collected from ripple cross laminations, clast imbrication,
215 and cross-bed and foreset plane measurements. Facies associations for both fan deltas are
216 constructed from combinations of identified facies, which are presented in correspondence
217 with those of Backert et al. (2010) for Kerinitis in Table A in the supplementary material.
218 Correlation of key stratigraphic surfaces was carried out by walking out beds and surfaces, by
219 annotations of photopanels in the field, and by using UAV photogrammetry-based 3D outcrop
220 models in Agisoft Photoscan software.

221 ### 4.2. Trajectory analysis

222 Trajectory analysis of the topset-foreset breakpoint (TFBP) was undertaken at both fan deltas
223 for the accessible middle units: 4-8 at Kerinitis and 7-11 at Selinous. The position of the TFBP
224 is identified from the transition from flat-lying topsets to steeply-dipping foresets. In
225 inaccessible locations, 3D outcrop models are used to identify the TFBP and assess the spatial
226 continuity of stratal surfaces across which the breakpoint moves. If the TFBP is not seen
227 directly, it is inferred from environmental transitions between down-dip outcrops at the same
228 stratigraphic level. It should be noted that the trajectory analysis undertaken of units at
229 Kerinitis are not correlatable to those analysed at Selinous.

230 ### 4.3. Numerical modelling with Syn-Strat

231 In order to refine the quantification of controlling parameters in the basin, we use a 3D
232 sequence stratigraphic forward model, Syn-Strat (Barrett et al., 2018). Syn-Strat produces a
233 3D graphical surface representing accommodation in the hangingwall of a normal fault,
234 resulting from spatially- and temporally-variable, tectonic subsidence, sedimentation and
235 base level inputs. Syn-Strat constructs this surface by combining one-dimensional graphical
236 curves that represent each control in time and space. Each parameter is defined along the
237 fault, away from the fault and in time. In this study, we plot accommodation along the fault
238 (x) and in time (y), for a given distance away from the fault. Stacking patterns or systems tracts
239 are then applied to the surface with colours. In this study, we subdivide the relative base level
240 curve with a falling limb and shorter periods of lowstand, transgression and highstand on the
241 rising limb. This resembles the sequence stratigraphic scheme used by Frazier (1974) and
242 Galloway (1989), and termed 'genetic sequence' by Catuneanu et al. (2009).

243 Previously, the model was used to demonstrate the sensitivity of sequence architecture to
244 multiple hypothetical control scenarios, including different relative control magnitudes,
245 subsidence rate regimes and sedimentation distribution models. Key outcomes were the
246 quantitative constraint of along-strike variation in stacking pattern, and of the nature of
247 diachroneity of sequence boundaries and maximum flooding surfaces (Barrett et al., 2018).
248 Here, we input real control parameters derived from field observations and trajectory
249 analyses. We refine the least certain control parameter (amplitude of base level change) with
250 a number of discrete tests, whilst keeping all other control parameters constant, by
251 comparing the modelled output with field observations. The test set-up and results are
252 presented in section 8.1.

253 5. SEDIMENTARY FACIES ANALYSIS RESULTS

254 The central parts of the fan deltas are the focus of sedimentological descriptions and
255 interpretations, where the topset-foreset transition records base level change and the
256 relative influence of accommodation and sediment supply. At Selinous, three down-dip
257 locations over ~800 m distance, covering the middle-to-upper units of the fan delta were
258 studied: S1 - Units 7 and 8, S2 - Units 8 and 9, and S3 - Units 10 and 11. At Kerinitis, our study
259 also focuses on three down-dip locations over ~700 m, covering the lower-middle units of the
260 delta: K1a, b, c - Units 4 and 7, K2 - Units 5 and 6, and K3 - Units 2 and 3. These are presented
261 on the 3D outcrop models in Fig. 4, but are not constrained as time-equivalent units.
262 Sedimentary facies characteristics are similar between the Selinous and Kerinitis fan deltas.
263 Eighteen sedimentary facies have been identified: six conglomeratic facies (abbreviated as
264 'Co'), six sandy facies (abbreviated as 'Sa') and six finer facies comprising mudstones and
265 siltstones (abbreviated as 'Fi'). Detailed facies descriptions are provided in Table A in the
266 Appendix and further facies information on the Kerinitis fan delta can be found in Backert et
267 al. (2010). The facies have been organised into four facies associations (FA) (Figs. 5 and 6, and
268 Table 1) that are differentiated based on geometric position (denoted by number) and eight
269 sub-associations that are differentiated based on depositional environment (denoted by
270 letter). The fluvial and shallow water topset FAs (1a-b and 2a-b) and the foreset FA (3)
271 construct the main stratal units of the deltas. The bottomset FAs (4a-c) form the thinner, finer-
272 grained intervals between the units.

273 5.1. FA1 - Fluvial topsets

274 We identify two fluvial topset FAs with 1a) channel-fill and 1b) delta plain interpretations (Fig.
275 5). The channel-fill FA constructs the largest proportion of the fan delta topset deposits
276 (~95%). FA 1a is characterised in Unit 7 at Location S1 (Selinous) and in Unit 3 at Location K3
277 (Kerinitis) as a poorly-sorted, sandy gravel-cobble conglomerate with crude laminations and
278 clast imbrication. The clasts are sub-angular to sub-rounded and the bed bases are highly
279 erosional (facies Co1 and Co2 in Table A, Appendix). We interpret this deposit to be the
280 product of bedload transport in a high-energy fluvial flow regime.
281 The fan delta plain FA (1b) is characterised in Unit 8 at Location S2 (Selinous) (Figs. 4 and 5)
282 and at the top of Unit 2 at Location K3 (Kerinitis) as a poorly-sorted, sandy gravel-cobble
283 conglomerate (facies Co1, Sa2, Sa6 and Fi3 in Table A, Appendix). The cobbles are <10 cm
284 diameter and sub-angular, implying limited transport time from source to deposition. The

285 gravelly coarse sand beds present normal grading and contain cm-thick, red palaeosols,
286 indicating subaerial exposure.

287 5.2. FA2 - Shallow water topsets

288 Two shallow-water topset FAs have been identified: 2a) beach barrier and 2b) lower
289 shoreface (Fig. 5). The beach barrier FA (2a) is characterised at Location S3 (Selinous) by bi-
290 directional metre-scale cross-beds with well-sorted, open-framework, rounded and discoidal
291 pebbles (facies Co4 and Co5 in Table A, Appendix). This indicates textural maturity and
292 character typical of beach reworking (Fig. 5). FA 2a is present at the top of Unit 10 at Selinous
293 Location S3 and is overlain by a finer-grained interval and subsequently by the 10 m-scale
294 foresets of Unit 11 (Fig. 4). We have not observed FA 2a at Kerinitis, but Backert et al. (2010)
295 report a foreshore FA at the top of Unit 7. The lower shoreface FA is present in the lower part
296 of Unit 8 at Location S2 (Selinous) and comprises m-scale bi-directional, asymptotic cross-
297 beds resembling hummocky-cross stratification (facies Co5 in Table A, Appendix), typical of
298 storm reworking below fair weather wave base.

299 5.3. FA3 - Foresets

300 The foreset FA represents most of the down-dip parts of the exposed fan delta successions
301 (Figs. 1, 2 and 5). At Selinous, the foreset FA is apparent in Unit 8 at Location S1, Unit 9 at
302 Location S2, and Unit 11 at Location S3 (Fig. 4). At the Kerinitis study locations, the foreset FA
303 is apparent in Unit 7 at Location K1a, b and c and Unit 6 at K2. The foreset FA is represented
304 by steep, basinward-dipping (between 22° and 25°), 10-350 m high cross-beds. The cross-beds
305 comprise well-sorted, clast-supported (and sometimes open-framework), sub-rounded
306 cobble conglomerate with some inverse grading and many scours (facies Co3, Co4 and Sa4 in
307 Table A, Appendix). In some places, the conglomeratic foreset units are separated by
308 preserved, gently-dipping finer-grained intervals (e.g. Fig. 5), but in most cases these are
309 eroded. The foreset facies association was emplaced in a high energy environment occupied
310 by avalanching sediment gravity flows, characteristic of the upper foreset slope. The height
311 of the foresets indicates the palaeo-water depth and ranges from a few metres when the
312 foresets built over a previous delta topset (e.g. S1-3; Fig. 4), to a few hundred metres, when
313 they built beyond the previous fan delta TFBP and into the deep water basin (e.g. Figs. 5 and
314 7).

315 5.4. FA4 - Bottomsets

316 Three bottomset FAs have been identified across the fan deltas and are interpreted to
317 represent distal (4a), intermediate (4b) and proximal (4c) positions with respect to the
318 sediment input point (Fig. 6 and Table 1). These deposits form the fine-grained intervals
319 between the major stratigraphic units.
320 The distal bottomset FA (4a) is mainly represented by calcareous mudstone-siltstone (marl)
321 beds, and is apparent in the interval between Units 7 and 8 at Location S1 (Selinous; Figs. 4
322 and 6). There is evidence of soft-sediment deformation and cm-wide, 10 cm-length, sand- and
323 mud-filled burrows (facies Sa1, Sa3, Fi1, Fi2 and Fi4, in Table A, Appendix). A 0.8 m thick,
324 laterally discontinuous, poorly-sorted, clast-supported sandstone-cobble-grade
325 conglomerate (facies Co4 in Table A, Appendix) cuts into the finer sediments. We interpret
326 the fine sediments to be deposited from dilute turbidity currents and suspension fall-out in a
327 low energy environment, and the conglomerate as a debrite sourced from the delta front.
328 The intermediate bottomset FA (4b) is evident between Units 10 and 11 at Location S3 (Figs.
329 4 and 6). It is characterised by interbedded sandstone and mudstone beds with some wavy
330 laminations. The sandstones are inversely graded with slightly erosive bases and gravel lags
331 (facies Sa1, Sa2, Sa4, Sa5, Fi1, Fi2, Fi3, Fi5 and Fi6 in Table A, Appendix), and are interpreted
332 as turbidites. Muddy intervals represent periods of quiescence between events, or dilute
333 turbidity current deposits. The proximal bottomset FA (4c) is observed between Units 8 and
334 9 at Location S2, between Units 5 and 6 at Location K2, and between Units 4 and 7 at Location
335 K1a (Figs. 4 and 6). It is characterised by coarser, mainly well-sorted sand-gravel-grade
336 sediments (facies Co6, Sa1-6, Fi1 and Fi2 in Table A, Appendix), with symmetrical and
337 asymmetrical ripple laminations, gravel dune-scale cross-beds, wavy and planar laminations,
338 soft sediment deformation (convolute laminations, folds and dewatering structures) and
339 bioturbation. The range of structures is interpreted to be due to a more proximal position
340 with respect to the river outlet, where hyperpycnal flows and wave processes may have
341 operated near the base of small foreset slopes in shallow water.

342

343 ## 6. KEY SURFACES

344 ### 6.1. Flooding surfaces

345 Fan delta successions can be subdivided into major stratal units based on stratal terminations
346 (e.g. downlaps, onlaps, and truncations) and major facies changes (Mitchum et al., 1977).

347 Fine-grained intervals are present between conglomeratic units in the topset regions and
348 transition zones. Basinward, fine-grained units are poorly preserved, with one exception at
349 Location K1b (Kerinitis). However, their correlative expression can be traced down-dip into
350 the foreset region using onlap and downlap patterns, and dip changes between foresets. In
351 both fan deltas, the fine-grained intervals are similar in their position (generally preserved in
352 the topset regions and transition zones) and thickness (~2 m). Locally, the bases of the fine-
353 grained intervals are slightly erosional. The facies of the fine-grained intervals range from
354 laminated mudstones and deformed siltstones (FA 4a), interbedded siltstones-sandstones (FA
355 4b), to rippled sandstones and gravels (FA 4c).

356 The base of the fine-grained intervals are interpreted to represent transgressive surfaces. The
357 maximum flooding surfaces are speculated to be within the fine-grained units in the topset
358 region of the deltas above each transgressive surface. The upper part of the fine-grained
359 intervals may be contemporaneous with the foreset progradation and therefore represent
360 the subsequent regressive trend. In the analogous modern conglomeratic deltas along the
361 southern shore of the Gulf of Corinth, fine-grained deposits are restricted to: 1) inter-
362 distributary bays, 2) lagoons, 3) fluvial overbanks, and 4) shelfal, shallow water bottomsets,
363 away from the dynamic, coarse-grained, gravity-driven processes in the foreset region, and
364 where dilute turbidity currents and suspension fall-out processes dominate. The two former
365 interpretations are omitted based on the absence of rootlets, palaeosols, intact fauna or
366 overall palaeocurrent changes that would indicate delta lobe avulsion and thus a migration
367 to an inter-distributary bay setting. In addition, the fine-grained intervals are too widespread
368 to represent a single lagoon in this setting. In the more proximal parts of the fan delta, it is
369 not possible to characterise the fine-grained intervals, so it is possible that they could
370 comprise of fluvial overbank deposits (Backert et al., 2010). However, an interpretation of
371 transgressive reworking of the topset region and deposition of shelfal fines is favoured.
372 We do not infer a great water depth for the deposition of the bottomset facies, and interpret
373 the fine-grained deposits to represent shelfal fines as opposed to slope/abyssal plain fines
374 when positioned landward of the large, basinward-dipping foresets. Where small foresets
375 prograde in shallow water in the proximal topset region, widespread bottomset deposition
376 over the previous fan delta topset occurs (Fig. 7). If the previous delta topset, and thus the
377 subsequent overlying bottomset, lies at a water depth above storm wave base, upper and

lower shoreface environmental facies are possible, even though geometrically they were deposited in the bottomsets (FA4b and FA4c). Bathymetry data of the Late Pleistocene and modern Selinous deltas (Cotterill, 2002; McNeill et al., 2005; Fig. 7) support the intercalation of bottomset and topset deposits. The topset of the Late Pleistocene delta (Y in Fig. 7) is overlain by the fine sediment of the modern system's bottomset (X in Fig. 7). Debrites from the modern system are identified in the bottomset of X that are placed on the topset of Y.

6.2. Sequence boundaries

In most cases, there is evidence for minor erosion of the fine-grained intervals by overlying topset units during progradation. However, deeper erosion (at the scale of several metres depth) that is subaerial in nature is only expressed at Selinous. At Selinous Location S2, the progradational foresets of Unit 9 infill a ~4 m deep erosional surface that incises into the underlying fine-grained interval. Where the fine-grained interval is missing, foresets are seen to directly overlay Unit 8, which comprises fluvial delta plain facies (FA1b) with several palaeosols (Fig. 8). The large lateral extent of the surface, traceable across the length of the whole fan delta, and the basinward shift of depositional environments, supports an interpretation of the erosive surface as a sequence boundary formed by a relative base level fall. Between Units 7 and 8 at S1, another surface with erosion of several metres depth is apparent and could be a sequence boundary. The bottomset deposit at this location is finer, and therefore interpreted to be more distal, than those at S2.

At Kerinitis, there is a ~100 m deep erosional cut at Key Stratal Surface 5 (KSS5) between the foresets of Units 3 and 7. Backert et al. (2010) attribute this to a large-scale submarine mass failure unrelated to relative base level change. Otherwise, major surfaces at Kerinitis appear to be either: 1) associated with major facies changes with limited erosion, or 2) erosive with a lack of subaerial indicators and occurring at the base of foresets ('cuspate erosion surfaces' in Backert et al., 2010). Therefore, these erosion surfaces are not interpreted to represent sequence boundaries due to the lack of evidence of subaerial exposure. We interpret that the erosion surfaces form by autocyclic processes, in agreement with the interpretation from Backert et al. (2010). Figure 8 shows the difference in the nature of key stratigraphic surfaces between Selinous (erosive sequence boundary) and Kerinitis (non-erosive surface) with examples from S2 and K3.

In summary, sequence boundaries are interpreted near the fault tip at Selinous, but not near the fault centre at Kerinitis. One explanation is that Kerinitis is positioned near the fault centre where greater subsidence could counteract basinwide relative base level falls (cf. Gawthorpe et al., 1994).

7. STRATAL STACKING PATTERNS

7.1. Description of stratal stacking patterns

At both fan deltas, the major stratal units are dominated by conglomerates, comprising FA 1 and 2 in the topsets and FA 3 in the foresets. The topsets extend for up to 2 km away from the fault to the TFBP, where restored stratigraphic dips increase from sub-horizontal to 20-25°. Average unit thickness is thinner at Selinous (~25 m) at Selinous compared to Kerinitis (~60 m). At both fan deltas, the units thicken towards the fault by ca. 10 m. The thickness of the units are generally uniform through time at Selinous. At Kerinitis, unit thickness generally increases towards the middle part of the fan delta and thins towards the top (Backert et al., 2010). The units also thicken into the foreset regions down-dip with foreset heights reaching >350 m, as the fan deltas prograded into deeper water depths towards the basin centre. At Selinous, we observe fifteen stratal units. At Kerinitis, we observe eleven stratal units, but the base of the Kerinitis succession is not observed. Previously, Kerinitis has been subdivided into twelve (Dart et al., 1994) or eleven stratigraphic units, with the uppermost unit designated as the Kolokotronis fan delta of the Upper Group (Backert et al., 2010). A 'proto-delta' (Stratal Unit 0 in Backert et al., 2010) recording initiation of subsidence is also identified towards the base of Kerinitis and is differentiated based on the interpretation of a sequence boundary at the top, drainage realignment and basinward shift of the subsequent units (Backert et al., 2010).

Trajectory analysis of the TFBP (Figs. 7 and 9) was undertaken at both fan deltas for the middle units: Units 4-8 at Kerinitis and Units 7-11 at Selinous. It should be noted that these units were chosen for analysis based on accessibility alone and there is no evidence for correlation between the units. Trajectory analysis for the whole of the Kerinitis fan delta is presented by Backert et al. (2010). Figure 9 shows schematic dip sections of the two fan deltas juxtaposed along the P-M Fault, with the trajectory analysis of each for comparison. The unit thicknesses are normalised to emphasise the relative patterns in the trajectory styles. From the trajectory

analysis, it appears that the stacking patterns are similar at both fan deltas across three scales, from stacking within units (10 m-scale), stacking between units (100 m-scale), to stacking of the whole fan delta succession (several 100 m-scale).

At Selinous, there is a progradational-to-aggradational style within Units 7-10, as shown by the climbing basinward trajectory of the TFBP. Unit 11 has a different trajectory, as small-scale (10 m) foresets are apparent closer to the fault. This is shown by the proximal climbing basinward trajectory of the TFBP (aggrading), followed by the horizontal basinward trajectory (prograding). Between Units 7 and 11 at Selinous there is generally retrogradation, i.e. the final TFBP of each unit is landward of that of the previous unit (Fig. 9). However, the Selinous fan delta is aggradational given the overall limited horizontal migration of the TFBP. Within Units 4-8 at Kerinitis, there appears to be a progradational-aggradational stacking pattern that resembles the style of Units 7-11 at Selinous. The final TFBP of Unit 5 is landward of that of Unit 4, indicating a phase of retrogradation. The final TFBP of Units 6 and 7 are basinward of their underlying units, indicating a phase of retrogradation. Finally, Unit 8 is landward of that of Unit 7, and indicates retrogradation. Backert et al. (2010) compile the fan delta units into three packages and interpret the lower package (Units 1-3) as progradational, the middle package as progradation-aggradational (Units 4-9) and the upper package as progradational (Units 10-11). Although there are variations in stacking pattern, the overall position of the TFBP between Units 4 and 8, and indeed of the whole fan delta, migrated a limited distance (~1.5 km; Fig. 9). Therefore, Kerinitis also exhibits an overall aggradational stacking pattern. It is not possible to access and characterise the fine-grained intervals across much of the topset part of the fan deltas with some exceptions, so it is not possible to define the landward extent of flooding.

7.2. Interpretation of stratal stacking patterns

The progradation-aggradation within the units at both fan deltas was a response to building out into space created by base level rise and subsidence, with sedimentation initially exceeding and then keeping pace with space creation. The retrogradational phase at Selinous, between Units 7-11, represents a time when the relative base level rise outpaced the sedimentation rate. The aggradational phase at Kerinitis between Units 4-8 represents a time when sedimentation was equal to the space available. The overall aggradational trend observed in both fan deltas is a response to overall sedimentation having kept pace with

accommodation generation. The greater unit thickness in the topset region at Kerinitis than Selinous may be attributed to the greater space made available from a higher subsidence rate near the fault centre than near the fault tip.

At both fan deltas there is clear cyclicity, with several major conglomeratic stratal units separated by fine-grained intervals, both with relatively constant thickness within each fan delta. Autocyclic switching of channel position is intrinsic to the architecture of fan delta tops. However, based on previous studies and repeated airborne photography of the Gulf of Corinth over the last 75 years, it is apparent that the rivers on the delta tops avulse on a decadal-centennial timescales (Soter & Katsonopoulou, 1998; McNeill & Collier, 2004). Here we are characterising an assumed larger scale cyclical behaviour. Such organised cyclicity is unlikely to develop from clustering of seismic activity (Scholz, 2010) as the long term velocity field over this timescale of 10-100 kyr is constant, due to the viscous flow of the lower crust (Wdowinski et al., 1989). Given this, and the fact that low-mid latitude Pleistocene lakes are characterised by high amplitude base level fluctuations (Gasse et al., 1989; Benson et al., 1998; Marshall et al., 2011; Lyons et al., 2015; Marchegiano et al., 2017), the cyclicity is attributed to periodicity in lake level change associated with climate. Previous authors also advocate this interpretation (Dart et al., 1994; Backert et al., 2010). Sediment supply is also likely to fluctuate with climate (Collier et al., 1990; Collier et al., 2000). Therefore, during the existence of the lake, climatic changes associated with orbital forcing influenced the evolution of the coast through fluctuations in both base level and sediment supply (Collier, 1990; Leeder et al., 1998; Moretti et al., 2004; Gawthorpe et al., 2017b). Lake level is interpreted to have risen and fallen multiple times throughout the Early-Middle Pleistocene with close to zero net change over the build times of the fan deltas. Without the addition of fault-related subsidence, there would be no space for the sediments to accumulate on the topsets, as each base level fall would remove the space created by each base level rise. Instead, distinctly progradational stacking pattern would be apparent with a consistent sediment supply, which is not apparent. Sedimentation must therefore have kept pace with the space creation from subsidence.

8. QUANTIFICATION OF CONTROLS

Here, we attempt to use the field data to discern and quantify the architectural controls on fan delta evolution. Subsidence rates can be estimated using the thickness of the syn-rift

503 successions over the time through which the fan deltas built (fan delta build time),
504 sedimentation rates from the combination of thickness accumulated and stacking pattern
505 over time, and base level change from extrapolation of unit thickness to the fault tip where
506 subsidence is zero. We assign qualitative uncertainty values (1-5) to each control parameter,
507 where 1 represents a very low uncertainty estimate and 5 represents a very high uncertainty
508 estimate. This approach identified which variable is most uncertain and would be a focus for
509 numerical model testing. Table 2 presents each control parameter and uncertainty estimate.
510 Local climate varied in response to orbital forcing during the Early-Middle Pleistocene with
511 the ~41 kyr dominant cyclicity (Capraro et al., 2005; Dodonov, 2005; Suc & Popescu, 2005)
512 that is recorded worldwide (Emiliani, 1978; Head & Gibbard, 2005; Lisiecki & Raymo, 2007).
513 This is assigned a low uncertainty value of 1. The Gulf of Corinth was mainly lacustrine (Lake
514 Corinth) between ~3.6 Ma and ~600 ka (Freyberg, 1973; Collier, 1990; Moretti et al., 2004;
515 Gawthorpe et al., 2017b). It is likely that lake levels fluctuated as a result of the well-
516 constrained cyclical climatic changes, but it is not known how the lake level changed and
517 whether it mimicked global sea level fluctuations. Various studies from the Late Pleistocene
518 show low-mid latitude lakes fluctuating with the same periodicity as global sea level, e.g. Lake
519 Lisan, Dead Sea (Torfstein et al., 2013), Lakes Tana and Tanganyika, East Africa (Gasse et al.,
520 1989; Marshall et al., 2011), Mono and Owens Lakes, California (Benson et al., 1998), Lake
521 Trasimeno, Italy (Marchegiano et al., 2017), with low lake levels corresponding to events
522 during glacial periods (low global sea level). However, the climate response (precipitation-
523 evaporation balance) to such events is spatially variable and it is also unknown whether this
524 Late Pleistocene trend is representative of climate changes during the Early-Middle
525 Pleistocene. The cyclical stratigraphy and facies of the deltas indicate that lake level changes
526 did occur, and a frequency of ~41 kyr in line with climate during the Early-Middle Pleistocene
527 is consistent with the age of the fan deltas.
528 Palynological data from the adjacent and contemporaneous Vouraikos delta indicate that the
529 fan deltas started to build at ~1.8 Ma (Ford et al., 2007), and stopped developing when they
530 began to be uplifted in the footwall of the West Helike Fault. Using uplift rates on the
531 contiguous East Helike Fault of 1-1.5 mm/yr (De Martini et al., 2004) and present-day final
532 topset elevation (~800 m) of the fan delta, an age for their demise is estimated as 530-800 ka
533 (Ford et al., 2007). The age constraint from palynology and uplift rates of ~1.8-~700 ka
534 supports the use of ~41 kyr as the dominant cyclicity.

Assuming the cyclicity is not autogenic, and each fine-grained interval contains a maximum flooding surface on the rising limb of a relative base level curve, the deposition of each unit represents one climatic cycle. At Selinous, there are fifteen stratal units, each representing ~41 kyr of deposition, from which we infer that the fan delta built over a total of 615 kyr. At Kerinitis, the base is not exposed, but there are at least eleven stratal units and so the minimum delta build time is 450 kyr. If the 'proto-delta' at the base were to be included in our framework or the lower units were exposed, this estimated build time would be longer. These approximations are consistent with previous estimates of fan delta build time based on palynological analysis of the concurrent and adjacent Vouraikos fan delta of 500-800 kyr (Malarte et al., 2004; Ford et al., 2007), and therefore we assign these build time estimates with a low uncertainty value of 2.

There is far greater uncertainty on the amplitude of lake level change. The unit thicknesses at Kerinitis are ~60 m and at Selinous are ~25 m. As both fan deltas developed only 6 km apart, in the hangingwall of the same fault, the lake level fluctuations affecting both systems were the same, and the difference in unit thicknesses is mainly due to variation in local subsidence rate. Subsidence was greater at Kerinitis than at Selinous; at least 35 m of unit thickness accounts for the contribution from additional subsidence at Kerinitis. Therefore, the maximum base level rise during one cycle is 25 m. As Selinous sits close to the fault tip but still underwent subsidence, lake level change would have been less than 25 m. The amplitude of lake level rise is assigned a high uncertainty value of 4.

Neither succession has undergone significant burial or compaction. The thickness of syn-rift sediments against the fault, and therefore maximum total subsidence at Selinous is ~400 m. The sediment is inferred to have accumulated over 615 kyr, which gives an average subsidence rate of 0.65 m/kyr. At Kerinitis, there is an estimated thickness, and therefore estimated total subsidence of ~800 m, which is calculated based on average topset unit thickness of 65 m, average topset thickening into the fault of ~10 m and 11 observable units. We infer that the sediment accumulated during 11 cycles over at least 450 kyr, which gives a minimum average subsidence rate of 1.77 m/kyr. The axes of the two fan deltas are positioned 6 km apart along-strike of the fault, and therefore using the two estimated average subsidence rates, subsidence decay per kilometre is approximately 0.19 m/kyr towards the fault tip. As Kerinitis is positioned is 10 km from the western fault tip and the fault is ~24 km in length, it sits ~2 km to the east of the fault centre, and therefore the average subsidence

rate there is slightly lower than the maximum on the fault. The Vouraikos fan delta sits ~3-4 km to the west of the fault centre and has a thickness of >800m (Ford et al., 2007). Extrapolating the subsidence decay rate derived between Selinous and Kerinitis towards the fault centre gives an estimated average minimum subsidence rate at the centre of the fault of 2.15 m/kyr. This estimate is highly comparable to Holocene fault-related subsidence rates from the Gulf of Corinth (2.2-3.5 mm/yr, McNeill & Collier, 2004), the Gulf of Patras, central Greece (average of 2-5 mm/yr, and 1-2 mm/yr away from the main border faults, Chronis et al., 1991) and the Wasatch Fault Zone, Basin and Range Province, USA (<2 mm/yr, Schwartz & Coppersmith, 1984; Machette et al., 1991; Gawthorpe et al., 1994). The syn-rift sediment thicknesses (total subsidence) is well-constrained and we consider the fan delta build time has relatively low uncertainty, hence the subsidence rates are assigned an equivalent low uncertainty value of 2. If each cycle had a ~20 kyr or ~100 kyr period, then the calculated subsidence rate would change, but this is neither consistent with the current understanding of climate in Greece in the Early-Middle Pleistocene, nor typical fault displacement rates in the region (McNeill & Collier, 2004; Capraro et al., 2005; Dodonov, 2005; Suc & Popescu, 2005).

The aggradational stacking trend at both fan deltas reveals that overall sedimentation rate kept pace with subsidence rate over the fan delta build times. Accordingly, as aggradation is present at both fan deltas and there is greater subsidence at Kerinitis, the sedimentation rate must be higher at Kerinitis. By dividing the total thickness of syn-rift sediment by the time taken for the sediment to accumulate, the average sedimentation rate at Selinous must be ~0.65 m/kyr, and at Kerinitis the average sedimentation rate is higher at ~1.77 m/kyr. This is similar to estimates for the Vouraikos fan delta that sits along-strike from Kerinitis (Fig. 1), where sedimentation rates are estimated to be 1.3-2 mm/yr (Ford et al., 2007). We refer to a sedimentation rate, and not a sediment supply rate, as some of the sediment may have been bypassed to the deep basin (e.g. Stevenson et al., 2015), or redistributed along-strike. Although justified as an estimate, an average sedimentation rate does not reflect any probable variation over the fan delta build time, for example from climate or slip rate related changes in erosion rate, we therefore assign these a high uncertainty value of 4.

9. REDUCING UNCERTAINTY OF CONTROL PARAMETERS

9.1. Numerical modelling with Syn-Strat

598 To reduce the uncertainty and more accurately quantify the major controls, we undertake a
599 numerical modelling exercise using Syn-Strat (Barrett et al., 2018). Syn-Strat produces a 3D
600 graphical surface representing accommodation in the hangingwall of a normal fault, resulting
601 from tectonic subsidence, sedimentation and sea- or lake-level inputs. Stacking patterns or
602 systems tracts can be applied to the surface. Control parameters that have been derived from
603 the field data are input into the model (Fig. 10). Various sensitivity tests are performed,
604 whereby one of the controls with the least uncertainty is varied to assess the closest match
605 to the field observations. Magnitude of base level change and sedimentation rate have the
606 greatest uncertainty (Table 2). Although the variation in sedimentation rate through time is
607 unknown, we have some constraint on average sedimentation rate from the aggradational
608 stacking patterns at both fan deltas. Lake level change amplitude was tested, and is varied at
609 5 m intervals from 5 m to 30 m (Fig. 11). The field observations that we compare are the
610 presence of sequence boundaries at Selinous and absence at Kerinitis, and are taken from
611 sections cutting the eastern margins of the fan deltas (positions are indicated on the flattened
612 plots, CI-CVI in Fig. 11 by the dashed lines).
613 Figure 10 explains the set-up of the numerical modelling tests. The size of the basin is defined
614 first in the model and represented by the size of the matrix. In this case, we define the fault
615 block width (6 km) and length (24 km), and the distance between the axis of each fan delta (6
616 km). The sediment input points are placed at the respective positions of the fan deltas along
617 the fault; 4 km (Selinous) and 10 km (Kerinitis) from the western fault tip. For the timescale,
618 we take the maximum fan delta build time, which is derived from Selinous as 615 kyr. Each
619 parameter is defined with one dimensional graphical curves plotted along the fault (x), away
620 from the fault (y), and in time (t) (Fig. 10A1).
621 We present the subsidence and lake level controls alone (Fig. 10A), in order to show the
622 resultant relative base level curve without sedimentation inputs. All parameters are kept
623 constant, other than the parameter in question (lake level amplitude). The 3D output shows
624 relative base level change at every point along the length of the fault for a position in the
625 immediate hangingwall of the fault (red line on the schematic diagram in B2 of Fig. 10). This
626 position is chosen as it is where the maximum topset unit thickness is observed and has been
627 used to calculate the subsidence and sedimentation rates. Systems tracts (or stages of a base
628 level curve) can be applied to a 3D relative base level (A2 and A3 of Fig. 10), just as they can
629 to a traditional 1D relative base level curve. With the given parameters, it is apparent that the

key stratigraphic surfaces are diachronous along the fault due to the subsidence variation. The falling limb of the relative base level curve (purple segment on Fig. 10A) and therefore sequence boundary is defined as the onset of the fall (between yellow and purple segments). It is not expressed at the fault centre, because subsidence outpaces the maximum rate of lake level fall. Sedimentation fills the space made available through time (Fig. 10B), so that at each time step, the space for subsequent deposition is a result of the preceding base level change, subsidence and sedimentation (Barrett et al., 2018). The addition of the sedimentation curves in time and space (Fig. 10B1) produces an accommodation curve that is reduced from sediment-filling at the positions of the fan deltas (Fig. 10B3).

The suite of sensitivity tests show that the diachroneity of stratigraphic surfaces decreases with increasing amplitude of base level, as the subsidence control becomes less dominant (Fig. 11). In the test with the lowest base level change (5 m; CI), the onset of relative base level fall occurs ~6-12 kyr earlier at the centre of the fan deltas than at the margins, whereas in the highest amplitude base level change test (30 m; CVI), it appears to occur at the same time along the fault, and any diachroneity is below the resolution of the model. There is a clear difference in the nature of sequence boundaries diachroneity between the tests. There are also changes within each test through time. It appears that the diachroneity generally increases through time and in doing so, progressively limits the sequence boundaries to positions closer towards the centre of the fan deltas. This is likely to be in response to the subsidence and sedimentation rates increasing through time in the model (Fig. 10). Our analysis was undertaken in the middle to upper units of the fan deltas and so it is here in the model outputs that we assess the presence or absence of sequence boundaries.

When the amplitude of base level change is >20 m (Fig. 11, CIV, CV and CVI), sequence boundaries are expressed across both Kerinitis and Selinous. In the field, however, we observe sequence boundaries at Selinous, but not at Kerinitis. In the 5 m amplitude test (Fig. 11, CI), sequence boundaries are present at the centre of both fan deltas as here there is maximum sedimentation; the sediments fill and exceed the available accommodation and this causes the system to prograde basinwards. However, at the margins of the fan deltas, where sedimentation is lower, the sequence boundaries are not expressed. As we observe sequence boundaries at the margin of Selinous, this test is also not comparable to our observations. For base level change amplitudes of 10 m and 15 m (Fig. 11, CII and CIII), sequence boundaries are expressed in the model results in the middle-upper units at the margin of Selinous, but

not at Kerinitis, which match our field observations. These tests are performed with average sedimentation rate equivalent to subsidence. Sedimentation rate is unlikely to be higher than our estimates, but could be lower. In this case, the effect of a relative base level rise would be amplified, so a lower lake level amplitude would be required to give the same response to match our field observations. The lake level change amplitude estimate is therefore a maximum value. In the 15 m amplitude change test (Fig 11, CIII), sequence boundaries are absent at Kerinitis in the upper units, but present in the middle units. In the field, the middle units (Units 4-8) do not reveal sequence boundaries, hence the 10 m amplitude lake level change amplitude is more consistent with field observations than the 15 m. However, we recognise that uncertainties in the inputs do not allow us to constrain the magnitude of lake level amplitude change to less than 5 m, henceforth we utilise a unit thickness extrapolation approach to validate the numerical modelling output.

9.2. Refinement of lake level change using unit thickness extrapolation method

Lake level changes of 10-15 m amplitude are supported by the extrapolation of unit thicknesses towards the fault tip (Fig. 12). Average unit thickness of the Kerinitis topsets is ~60 m and at Selinous is ~25 m. The thickness contribution from subsidence is at least 35 m at Kerinitis and reduces towards the fault tip (in blue on Fig. 12). The unit thickness decay between Kerinitis and Selinous occurs over 6 km, with a decay rate of 5.8 m/km. If the same assumed linear unit decay trend is extrapolated a further 4 km to the fault tip, where fault-controlled subsidence is theoretically zero, the units would hypothetically lose a further 23 m thickness, leaving 12 m of possible unit thickness at the fault tip. There must be a space created for this thickness of sediment to accumulate at the fault tip as subsidence is zero, and fluctuation of lake level associated with climate change is the most likely mechanism. There is no actual stratigraphy preserved at the fault tip because there is no net accommodation gain in the immediate hangingwall of the P-M Fault. This analysis assumes that there is no additional space creation from other nearby faults, background subsidence or underlying topography for the sediments to fill. The calculated 12 m base level change is comparable with the model estimate of 10-15 m.

10. IMPLICATIONS

The implications for this work are threefold: 1) we demonstrate a method for dissociating base level from faulting, which could be applied to a number of other rift basin-fills; 2) we present a quantitative modelling approach to the analysis of stacking and surfaces,

694 constrained by field data, that could be applied to stratigraphic pinchout assessment and
695 cross-hole correlations in reservoir analysis; and 3) we derive a lake level change amplitude
696 for the region, which could aid regional palaeoclimate studies and inform broader climate-
697 system models.

698 10.1. Applications to other basins

699 Two independent methods – forward modelling with Syn-Strat and unit thickness
700 extrapolation – provided comparable results for lake level change amplitude in Lake Corinth
701 through the Early to Middle Pleistocene (10-15 m). Other studies have presented the problem
702 of dissociating base level from faulting in rift basins. Dorsey & Umhoefer (2000) attribute the
703 accommodation creation for the Pliocene vertically stacked deltas in the Loreto Basin, Gulf of
704 California to episodic fault-controlled subsidence near the fault centre, and to eustasy near
705 the fault tip, by correlation of parasequences to a marine oxygen isotope curve. It is likely that
706 subsidence rate outpaced eustasy near the fault centre to restrict the development of
707 sequence boundaries to the fault tips. By utilising our methods, it would be possible to affirm
708 whether the stacking cyclicity observed is attributable to faulting or base level change. The
709 numerical modelling approach with Syn-Strat is not limited to rift basins. Any mechanism that
710 creates or reduces accommodation (e.g. salt diapirism or thrust folding) could replace the
711 normal fault in the model and sequence stratigraphic evolution in these settings could be
712 assessed. In areas with good age/eustatic sea level constraints, and for given sedimentation
713 rates, different structural styles could be tested to find the best fit to the observed
714 stratigraphy.

715 10.2. Subsurface appraisal

716 By comparing two fan deltas we have been able to constrain the interplay of allogenic controls
717 responsible for their depositional architectures. The study of a single fan delta would not have
718 been sufficient to do this, hence we highlight the importance of studying multiple systems
719 within a single basin-fill. With subsidence rates of 0.65 m/kyr at Selinous at ~4 km from the
720 western fault tip, 1.77 m/kyr at Kerinitis at ~10 km from the tip, there should be a maximum
721 subsidence rate of 2.14 m/kyr at the fault centre (~2 km further along-strike). Unit thickness
722 could, for instance, be extrapolated along-strike to provide a hypothetical estimate of 72 m
723 at the fault centre, assuming predominantly aggradational stacking geometries. We cannot
724 test this in the area as no fan delta is located exactly at the fault centre and there is no point
725 source at the fault tip. However, in other settings the ability to predict the variation of

726 stratigraphic thickness along-strike is important for assessment of stratigraphic pinchout in
727 hydrocarbon reservoirs. The modelling work also demonstrates the extent and nature of
728 diachroneity of sequence boundaries along-strike. Such spatiotemporal variability in erosion
729 can have implications for reservoir unit correlation and connectivity. Barrett et al. (2018)
730 demonstrate that the surfaces are not only diachronous, but how that diachroneity may
731 change along the fault and through time for given scenarios. Here, we go one step further and
732 quantify that variation. For example, in the 10 m lake level amplitude test, the sequence
733 boundary occurs ~6 kyr earlier at the centre of the fan deltas than at the margins (Fig. 11). In
734 a subsurface setting, this method could improve confidence in cross-hole correlations of these
735 surfaces.

736 10.3. Implications of a lake level change amplitude of 10-15 m

737 Early-Middle Pleistocene climate for the Mediterranean region has been studied using
738 palynology (e.g. Capraro et al., 2005; Suc & Popescu, 2005; Joannin et al., 2007) and
739 speleothem analysis as a proxy for local rainfall and air temperature (e.g. Dotsika et al., 2010).
740 Climate fluctuated between cold and dry, and warm and wet periods in association with
741 global climatic records during this time (Head & Gibbard, 2005, and references therein). We
742 interpret that these climate changes resulted in changes in the level of Lake Corinth, which
743 have been estimated to have an amplitude of 10-15 m. The geological record of amplitude is
744 a valuable resource and our estimated value could inform hydrological budget calculations in
745 both regional palaeoclimate studies of the Gulf of Corinth or Mediterranean, and broader
746 climate-system numerical models that require lake level data as an input. Numerical models
747 used to predict how future climate may impact a region require quantitative palaeoclimatic
748 data from multiple proxies from the land and ocean to understand the forcing mechanisms
749 behind observed climatic patterns, and also to validate and improve the models themselves
750 (Abrantes et al., 2012, Luterbacher et al., 2012).

751 The volume of water that a 10-15 m change in lake level represents is crudely calculated for
752 the Middle Pleistocene Lake Corinth. The lake boundaries are taken from Nixon et al. (2016)
753 and do not include the Alkyonides Basin that may have been disconnected at that time (Nixon
754 et al., 2016). A ~240 km perimeter is estimated and a volume change of ~17-26 km^3 (order of
755 10^{10} m^3). How a 10-15 m rise would have impacted the coastline is dependent on the coastal
756 gradient and local sediment supply. With an average gradient of the shelf slope in the Gulf of
757 Corinth of 2.8° (from the Alkyonides Basin, Leeder et al., 2002), a 10-15 m change in lake level

758 would cause the coastline to shift by 250-310 m. However, considering parts of the coastline
759 positioned on a fan delta, with topset gradients of <0.1° and foreset gradients of ~22°, this
760 shift would be highly variable, depending on whether there is a lake level rise or fall. Starting
761 at the topset-foreset breakpoint, a fall of 10-15 m, would cause the shoreline to advance only
762 25-40 m due to the steep foreset slope (not including effects on sediment supply). On the
763 other hand, a rise of 10-15 m from the breakpoint would cause a potential shoreline shift of
764 5-10 km, due to the near-horizontal (0.1°) topset. In reality, coastal topography and the
765 border faults would prevent such a dramatic shift, but this could explain the ~2.5-3 km extent
766 from the P-M Fault of the fine-grained intervals that contain the maximum flooding surfaces
767 between each major unit observed at both Selinous and Kerinitis.
768
769 11. CONCLUSIONS
770 We have undertaken the first sedimentological and stratigraphic study of the Selinous syn-rift
771 fan delta in the Gulf of Corinth, Greece, and made comparisons with the adjacent and
772 contemporaneous Kerinitis syn-rift fan delta. In doing so, we demonstrate that a multi-
773 system-study approach is an effective way of understanding and quantifying allogenic basin
774 controls. This is the first detailed comparison of stratigraphic architectures between along-
775 strike systems in the hangingwall of a normal fault, positioned near the fault centre and near
776 the fault tip. Eighteen facies and eight facies associations were identified between the deltas,
777 and distinguished in terms of their topset to bottomset geometric position and depositional
778 environments. Maximum flooding surfaces are apparent at both fan deltas between the
779 major stratal units, but sequence boundaries are only observed at Selinous, near the fault tip.
780 In spite of this, stacking patterns are similar between the fan deltas, as shown by trajectory
781 analyses of both, with evidence of: 1) progradation within the units (10 m-scale), 2)
782 retrogradation at Selinous and aggradation at Kerinitis between middle-upper units (100 m-
783 scale), 3) aggradation at the fan delta scale (400-800 m). This implies that overall
784 sedimentation kept pace with accommodation in both cases. As subsidence rate is lower at
785 Selinous near the fault tip, average sedimentation rate must also be lower there than at
786 Kerinitis. The duration for the whole of each fan delta to build were estimated - 615 kyr for
787 Selinous and at least 450 kyr for Kerinitis. Controlling parameters were quantified from field
788 observations, including subsidence and average sedimentation rates of 0.65 m/kyr at Selinous
789 and >1.77 m/kyr at Kerinitis, and assigned uncertainty values from 1-5. The amplitude of lake

level change through time was deemed the most uncertain parameter. Numerical modelling with Syn-Strat was undertaken using the presence of sequence boundaries at both localities in various scenarios, to reduce the uncertainty and better constrain the amplitude of lake level change. Lake level changes of 10-15 m were estimated from the model and supported by an independent calculation of 12 m from unit thickness extrapolation towards the fault tip. The study has three broad outcomes: 1) demonstration of two complementary methods to identify and quantify faulting and base level signals in the stratigraphic record, which could be applied to other rift basin-fills, 2) a quantitative approach to the analysis of stacking and surfaces, constrained by field data, that can be applied to stratigraphic pinchout assessment and cross-hole correlations in reservoir analysis; and 3) an estimate of lake level change amplitude in Lake Corinth for the Early-Middle Pleistocene, which could aid regional palaeoclimate studies and inform broader climate-system models.

12. ACKNOWLEDGMENTS

We thank the project sponsor, Neptune Energy, who support the SMRG (Shallow Marine Research Group). Barrett was partially sponsored by a VISTA Visiting Scholarship at the University of Bergen. Gawthorpe acknowledges support from the VISTA Professorship.

808 13. REFERENCES

809 ABRANTES, F., VOELKER, A.H.L., SIERRO, F.J., NAUGHTON, F., RODRIGUES, T., CACHO, I.,
810 ARIZTEGUI, D., BRAYSHAW, D., SICRE, M-A. & BATISTA, L. (2012) 1 – Paleoclimate variability
811 on the Mediterranean region. *The Climate of the Mediterranean Region, from the past to the*
812 *future, Elsevier, London.* 1-86pp.
813 AVALLONE, A., BRIOLE, P., AGATZA-BALODIMOU, A.M., BILLIRIS, H., CHARADE, O., MITSAKAKI,
814 C., NERCESSIAN, A., PAPAZISSI, K., PARADISSIS, D. & VEIS, G. (2004) Analysis of eleven years
815 of deformation measured by GPS in the Corinth Rift Laboratory area. *Comptes Rendus*
816 *Geoscience*, 336, 301-311.
817 BACKERT, N., FORD, M. & MALARTRE, F. (2010) Architecture and sedimentology of the
818 Kerinitis Gilbert-type fan delta, Corinth Rift, Greece. *Sedimentology*, 57, 543-586.
819 BARRETT, B., HODGSON, D.M., COLLIER, R.E.Ll. & DORRELL, R.M. (2018). Novel 3D sequence
820 stratigraphic numerical model for syn-rift basins: analysing architectural responses to eustasy,
821 sedimentation and tectonics. *Marine and Petroleum Geology,* 92, 270-284. doi:
822 10.1016/j.marpetgeo.2017.10.026.
823 BELL, R.E., MCNEILL, L.C., BULL, J.M. & HENSTOCK, T.J. (2008) Evolution of the offshore
824 western Gulf of Corinth. *Geol. Soc. Am. Bull.,* 120, 156-178.
825 BENSON, L.V., LUND, S.P., BURDETT, J.W., KASHGARIAN, M., ROSE, T.P., SMOOT, J.P. &
826 SCHWARTZ, M. (1998) Correlation of Late-Pleistocene Lake-Level Oscillations in Mono Lake,
827 California, with North Atlantic Climate Events. *Quaternary Research*, 49, 1-10.
828 BERNARD, P., LYON-CAEN, H., BRIOLE, P., DESCHAMPS, A., BOUDIN, F., MAKROPOULOS, K.,
829 PAPADIMITRIOUS, P., LEMEILLE, F., PATAU, G., BILLIRIS, H., PARADISSIS, D., PAPAZISSI, K.,
830 CASTAREDE, H., CHARADE, O., NERCESSIAN, A., AVALLONE, A., PACCHIANI, F., ZAHRADNIK, J.,
831 SACKS, S. & LINDE, A. (2006) Seismicity, deformation and seismic hazard in the western rift of
832 Corinth: new insights from the Corinth Rift Laboratory (CRL). *Tectonophysics,* 426, 7-30.
833 BRIOLE, P., RIGO, A., LYON-CAEN, H., RUEGG, J.C., PAPAZISSI, K., MITSAKAKI, C., BALODIMOU,
834 A., VEIS, G.*, et al.* (2000) Active deformation of the Corinth rift, Greece: Results from repeated
835 Global Positioning System surveys between 1990 and 1995. *Journal of Geophysical Research-*
836 *Solid Earth*, 105, 25605-25625.
837 CAPRARO, L., ASIOLI, A., BACKMAN, J., BERTOLDI, R., CHANNELL, J.E.T., MASSARI, F. & RIO, D.
838 (2005) Climatic patterns revealed by pollen and oxygen isotope records across the Matuyama-

839 Brunhes Boundary in the central Mediterranean (southern Italy). *Geological Society, London,*
840 *Special Publications,* 247, 159-182.
841 CATUNEANU, O., ABREU, V., BHATTACHARYA, J.P., BLUM, M.D., DALRYMPLE, R.W., ERIKSSON,
842 P.G., FIELDING, C.R., FISHER, W.L., GALLOWAY, W.E., GIBLING, M.R., GILES, K.A., HOLBROOK,
843 J.M., JORDAN, R., KENDALL, C.G.S.T.C., MACURDA, B., MARTINSEN, O.J., MIALL, A.D., NEAL,
844 J.E., NUMMEDAL, D., POMAR, L., POSAMENTIER, H.W., PRATT, B.R., SARG, J.F., SHANLEY,
845 K.W., STEEL, R.J., STRASSER, A., TUCKER, M.E., WINKER, C. (2009) Towards the standardization
846 of sequence stratigraphy. *Earth Sci. Rev.,* 92, 1–33.
847 CLARKE, P.J., DAVIES, R.R., ENGLAND, P.C., PARSONS, B.E., BILLIRIS, H., PARADISSIS, D., VEIS,
848 G., DENYS, P.H., CROSS, P.A., ASHKENAZI, V. & BINGLEY, R. (1997). Geodetic estimate of
849 seismic hazard in the Gulf of Korinthos. *Geophysical Research Letters*, 24, 1303-1306.
850 CHRONIS, G., PIPER, D. J. W. & ANAGNOSTOU, C. (1991) Late Quaternary evolution of the Gulf
851 of Patras, Greece: tectonism, deltaic sedimentation and sea-level change. *Marine Geology,*
852 97, 191-209.
853 COLLIER, R.E.Ll. (1990) Eustatic and tectonic controls upon Quaternary coastal sedimentation
854 in the Corinth Basin, Greece. *J. Geol. Soc.,* 147, 301-314.
855 COLLIER, R.E.Ll. & DART, C.J. (1991) Neogene to Quaternary rifting, sedimentation and uplift
856 in the Corinth Basin, Greece. *J. Geol. Soc. London*, 148, 1049-1065.
857 COLLIER, R.E.Ll., LEEDER, M.R. & MAYNARD, J.R. (1990) Transgressions and regressions: a
858 model for the influence of tectonic subsidence, deposition and eustasy, with application to
859 Quaternary and Carboniferous examples. *Geol. Mag.,* 127, 117-128.
860 COLLIER, R.E.Ll., LEEDER, M.R., TROUT, M., FERENTINOS, G., LYBERIS, E. & PAPATHEODOROU,
861 G. (2000) High sediment yields and cool, wet winters: test of last glacial paleoclimates in the
862 northern Mediterranean. *Geology*, 28, 999-1002.
863 COLLIER, R.E.Ll. & THOMPSON, J. (1991) Transverse and linear dunes in an Upper
864 Pleistocene marine sequence, Corinth Basin, Greece. *Sedimentology*, 38, 1021-1040.
865 COTTERILL, C.J. (2002). A high resolution Holocene fault activity history of the Aigion shelf,
866 Gulf of Corinth, Greece. PhD Thesis, School of Ocean and Earth Sciences, University of
867 Southampton, UK.
868 DART, C.J., COLLIER, R.E.L., GAWTHORPE, R.L., KELLER, J.V.A. & NICHOLS, G. (1994) Sequence
869 stratigraphy of (?)Pliocene-quaternary synrift, gilbert-type fan deltas, Northern
870 Peloponnesos, Greece. *Mar. Pet. Geol.,* 11, 545-560.

871 DE MARTINI, P., PANTOSTI, D., PALYVOS, N., LEMEILLE, F., MCNEILL, L. & COLLIER, R.E.Ll.
872 (2004) Slip rates of the Aigion and Eliki faults from uplifted marine terraces, Corinth Gulf,
873 Greece. *C. R. Geosci.,* 336, 325-334.
874 DODENOV, A.E. (2005) The stratigraphic transition and suggested boundary between the
875 Early and Middle Pleistocene in the loess record of northern Eurasia. *Geological Society,*
876 *London, Special Publications,* 247, 209-219.
877 DORSEY, R.J. & UMHOEFER, P.J. (2000) Tectonic and eustatic controls on sequence
878 stratigraphy of the Pliocene Loreto Basin, Baja California Sur, Mexico. *GSA Bull.,* 112, 177-199.
879 DORSEY, R.J., UMHOEFER, P.J. & RENNE, P.R. (1995) Rapid subsidence and stacked gilbert-
880 type fan deltas, Pliocene Loreto Basin, Baja California Sur, Mexico. *Sediment. Geol.,* 98, 181-
881 204.
882 DOTSIKA E., PSOMIADIS D., ZANCHETTA G., SPYROPOULOS N., LEONE G., TZAVIDOPOULOS I.
883 & POUTOUKIS D. (2010). Pleistocene palaeoclimatic evolution from Agios Georgios Cave
884 speleothem (Kilkis, N. Greece). Bulletin of the Geological Society of Greece, Proceedings of
885 the 12th International Congress, Patras, 2, 886-895.
886 EMILIANI, C. (1978) The cause of the ice ages. *Earth & Planetary Science Letters,* 37, 349-352.
887 FLOYD, M.A., BILLIRIS, H., PARADISSIS, D., VEIS, G., AVALLONE, A., BRIOLE, P., MCCLUSKY, S.,
888 NOCQUET, J.-M., PALAMARTCHOUK, K., PARSONS, B. & ENGLAND, P.C. (2010) A new velocity
889 field for Greece: implications for the kinematics and dynamics of the Aegean. Journal of
890 Geophysical Research, 115, B10403.
891 FORD, M., HEMELSDAEL, R., MANCINI, M. & PALYVOS, N. (2016) Rift migration and lateral
892 propagation: evolution of normal faults and sediment-routing systems of the western Corinth
893 rift (Greece). In: The Geometry of Normal Faults (Ed. by Childs C., Holdsworth R.E., Jackson
894 C.A-L., Manzocchi T., Walsh J.J., Yielding G.) *Geol. Soc. London, Spec. Publ.,* 439.
895 FORD, M., ROHAIS, S., WILLIAMS, E.A., BOURLANGE, S., JOUSSELIN, D., BACKERT, N. &
896 MALARTRE, F. (2013) Tectonosedimentary evolution of the western Corinth rift (Central
897 Greece). *Basin Research*, 25, 3-25.
898 FORD, M., WILLIAMS, E.A., MALARTRE, F. AND POPESCU, S.M. (2007) Stratigraphic
899 architecture, sedimentology and structure of the Vouraikos Gilbert-type fan delta, Gulf of
900 Corinth, Greece. In: Sedimentary Processes, Environments and Basins. A Tribute to Peter
901 Friend (Ed. by G. Nichols, E. Williams and C. Paola), *Int. Assoc. Sedimentol. Spec. Publ.,* 38, 49-
902 90.

903 FRAZIER, D. (1974) Depositional Episodes: Their Relationship to the Quaternary Stratigraphic
904 Framework in the Northwestern Portion of the Gulf Basin. Bureau of Economic Geology,
905 University of Texas, Geological Circular 74-1, pp. 26.
906 FREYBERG, B. VON (1973) Geologie des Isthmus von Korinth. *Erlanger Geologische*
907 *Abhandlungen, 95.* Junge und Sohn, Universitats-Buchdruckerei, Erlangen.
908 GALLOWAY, W.L. (1989) Genetic stratigraphic sequences in basin analysis I: architecture and
909 genesis of flooding surface bounded depositional units. *AAPG Bull.,* 73, 125–142.
910 GARCIA-GARCIA, F., FERNANDEZ, J., VISERAS, C. & SORIA, J.H. (2006) Architecture and
911 sedimentary facies evolution in a delta stack controlled by fault growth (Betic Cordillera,
912 southern Spain, late Tortorian). *Sed. Geol.,* 185, 79-92.
913 GARCIA-MONDÉJAR, J. (1990) Sequence analysis of a marine Gilbert-type delta, La Miel,
914 Albian Lunada Formation of northern Spain. In: Coarse-Grained Deltas (Ed. by A. Colella and
915 D.B. Prior), *Int. Assoc. Sedimentol. Spec. Publ.,* 10, 255-269.
916 GASSE, F., LÉDÉE, V., MASSAULT, M. & FONTES, J-C. (1989) Water-level fluctuations of Lake
917 Tanganyika in phase with oceanic changes during the last glaciation and deglaciation. *Nature*,
918 342, 57-59.
919 GAWTHORPE, R.L., ANDREWS, J.E., COLLIER, R.E.LI., FORD, M., HENSTRA, G.A., KRANIS, H.,
920 LEEDER, M.R., MURAVCHIK, M. & SKOURTSOS, E. (2017a) Building up or out? Disparate
921 sequence architectures along an active rift margin – Corinth rift, Greece. *Geology*, 45, 111-
922 114.
923 GAWTHORPE, R.L., FRASER, A. & COLLIER, R.E.LI. (1994) Sequence stratigraphy in active
924 extensional basins: implications for the interpretation of ancient basin fills. *Marine and*
925 *Petroleum Geology,* 11, 642-658.
926 GAWTHORPE, R.L., HARDY, S. & RITCHIE, B. (2003) Numerical modelling of depositional
927 sequences in half-graben rift basins. *Sedimentology*, 50, 169-185.
928 GAWTHORPE, R.L., LEEDER, M.R., KRANIS, H., SKOURTSOS, E., ANDREWS, J.E., HENSTRA, G.A.,
929 MURAVCHIK, M., TURNER, J.A. & STAMATAKIS, M. (2017b) Tectono-sedimentary evolution of
930 the Plio-Pleistocene Corinth rift, Greece. *Basin Res.,* 1-32, doi: 10.1111/bre.12260.
931 GAWTHORPE, R.L. & LEEDER, M.R. (2000) Tectono-sedimentary evolution of active
932 extensional basins. *Basin Res.,* 12, 195-218.
933 GAWTHORPE, R.L., SHARP, I., UNDERHILL, J.R. & GUPTA, S. (1997) Linked sequence
934 stratigraphic and structural evolution of propagating normal faults. *Geology,* 25, 795-798.

935 GHISETTI, F. & VEZZANI, L. (2004) Plio-Pleistocene sedimentation and fault segmentation in
936 the Gulf of Corinth (Greece) controlled by inherited structural fabric. *Comptes Rendus*
937 *Geosciences*, 336, 243-249.
938 GILBERT, G.K. (1885) The topographic features of lake shores. *US Geol. Surv. Ann. Rep.,* 5, 69-
939 123.
940 GILBERT, G.K. (1890) Lake Bonneville. *US Geol. Surv. Monogr.,* 1, 1-438.
941 GOLDSWORTHY, M. & JACKSON, J. (2001) Migration of activity within normal fault systems:
942 examples from the Quaternary of mainland Greece. *Journal of Structural Geology*, 23, 489-
943 506.
944 HARDY, S., DART, C.J. & WALTHAM, D. (1994) Computer modelling of the influence of
945 tectonics on sequence architecture of coarse-grained fan deltas. *Marine and Petroleum*
946 *Geology*, 11, 561-574.
947 HARDY, S. & GAWTHORPE, R.L. (1998) Effects of variations in fault slip rate on sequence
948 stratigraphy in fan deltas: insights from numerical modeling. *Geology,* 26, 911-914.
949 HARDY, S. & GAWTHORPE, R.L. (2002) Normal fault control on bedrock channel incision and
950 sediment supply: insights from numerical modeling. *Journal of Geophysical Research*, 107,
951 2246.
952 HEAD, M.J. & GIBBARD, E.L. (2005) Early-Middle Pleistocene Transitions: The Land-Ocean
953 Evidence. *Geological Society, London, Special Publications*, 247, 1-18.
954 JACKSON, C.A.L., GAWTHORPE, R.L., CARR, I.D. & SHARP, I.R. (2005) Normal faulting as a
955 control on the stratigraphic development of shallow marine syn-rift sequences: the Nukhul
956 and Lower Rudeis Formations, Hammam Faraun fault block, Suez Rift, Egypt. *Sedimentology,*
957 52, 313-338.
958 JERVEY, M.T. (1988) Quantitative geological modeling of siliciclastic rock sequences and their
959 seismic expression. In: Sea-Level Changes: An Integrated Approach (Ed. by C.K. Wilgus, B.S.
960 Hastings, C.G.St.C. Kendall, H.W. Posamentier, C.A. Ross. & J.C. Van Wagoner), *SEPM Special*
961 *Publications*, 42, 47-69.
962 JOANNIN, S., QUILLÉVÉRÉ, F., SUC, J-P., LÉCUYER, C. & MARTINEAU, F. (2007) Early Pleistocene
963 climate changes in the central Mediterranean region as inferred from integrated pollen and
964 planktonic foraminiferal stable isotope analyses. *Quaternary Research*, 67, 264-274.

965 LEEDER, M.R., MARK, D.F., GAWTHORPE, R.L., KRANIS, H., LOVELESS, S., PEDENTCHOUK, N.,
966 SKOURTSOS, E., TURNER, J., ANDREWS, J.E. & STAMATAKIS, M. (2012) A "Great Deepening":
967 Chronology of rift climax, Corinth rift, Greece. *Geology,* 40, 999-1002.
968 LEEDER, M.R., COLLIER, R.E.Ll., ABDUL AZIZ, L.H., TROUT, M., FERENTINOS, G.,
969 PAPATHEODOROU, G. & LYBERIS, E. (2002) Tectono-sedimentary processes along an active
970 marine/lacustrine half-graben margin: Alkyonides Gulf, E. Gulf of Corinth, Greece. *Basin*
971 *Research*, 14, 25-41.
972 LEEDER, M.R. & GAWTHORPE, R.L. (1987) Sedimentary models for extensional tilt block/half-
973 graben basins. In: Continental Extensional Tectonics (Ed. by M.P. Coward, J.F. Dewey & P.L.
974 Hancock), *Geological Society, London, Special Publications*, 28, 139-152.
975 LEEDER, M.R., HARRIS, T. AND KIRKBY, M.J. (1998) Sediment supply and climate change:
976 implications for basin stratigraphy. *Basin Res.,* 10, 7-18.
977 LEEDER, M.R., MACK, G.H., BRASIER, A.T., PARRISH, R.R., MINTOSH, W.C., ANDREWS, J.E. &
978 DUREMEIJER, C.E. (2008) Late-Pliocene timing of Corinth (Greece) rift-margin fault migration.
979 *Earth and Planetary Science Letters*, 274, 132-141.
980 LISIECKI, L.E. & RAYMO, M.E. (2007) Plio–Pleistocene climate evolution: trends and transitions
981 in glacial cycle dynamics. *Quaternary Science Reviews*, 26, 56-69.
982 LUTERBACHER, J., GARCÍA-HERRERA, R., AKCER-ON, S., ALLAN, R., ALVAREZ-CASTRO, M-C.,
983 BENITO, G., BOOTH, J., BÜNTGEN, U., CAGATAY, N., COLOMBAROLI, D., DAVIS, B., ESPER, J.,
984 ET AL. (2012) 2 – A review of 2000 years of paleoclimatic evidence in the Mediterranean. *The*
985 *Climate of the Mediterranean Region, from the past to the future, Elsevier, London.* 87-185pp.
986 LYONS, R.P., SCHOLTZ, C.A., COHEN, A.S., KING, J.W., BROWN, E.T., IVORY, S.J., JOHNSON, T.C.,
987 DEINO, A.L., REINTHAL, P.N., McGLUE, M.M. & BLOME, M.W. (2015) Continuous 1.3-million-
988 year record of East African hydroclimate, and implications for patterns of evolution and
989 biodiversity. *Proceedings of the National Academy of Sciences of the United States of America,*
990 112, 15568-15573.
991 MACHETTE, M. N., PERSOUNIUS, S. F. & NELSON, A. R. (1991) The Wasatch fault zone, Utah -
992 - segmentation and history of Holocene earthquakes. *J. Struct. Geol.,* 13, 137-149.
993 MALARTRE F., FORD M. & WILLIAMS E.A. (2004) Preliminary biostratigraphy and 3D
994 lithostratigraphy of the Vouraikos Gilbert-type fan delta. Implications for the evolution of the
995 Gulf of Corinth, Greece*. C.R. Geoscience*, 336, 269-280.

996 MARCHEGIANO, M., FRANCKE, A., GLIOZZI, E., ARIZTEGUI, D. (2017) Arid and humid phases in
997 central Italy during the Late Pleistocene revealed by the Lake Trasimeno ostracod record.
998 *Palaeogeography, Palaeoclimatology, Palaeoecology*, 490, 55-69.
999 MARSHALL, M.H., LAMB, H.F., HUWS, D., DAVIES, S.J., BATES, R., BLOEMENDAL, J., BOYLE, J.,
1000 LENG, M.J., UMER, M., BRYANT, C. (2011) Late Pleistocene and Holocene drought events at
1001 Lake Tana, the source of the Blue Nile. *Global and Planetary Change*, 78, 147-161.
1002 McNEILL, L.C & COLLIER, R.E.Ll. (2004) Uplift and slip rates of the eastern Eliki fault segment,
1003 Gulf of Corinth, Greece, inferred from Holocene and Pleistocene terraces. Journal of the
1004 Geological Society, London, 161, 81-92.
1005 McNEILL, L.C., COTTERILL, C.J., HENSTOCK, T.J., BULL, J.M., STEFATOS, A., COLLIER, R.,
1006 PAPATHEODEROU, G., FERENTINOS, G. & HICKS, S.E. (2005) Active faulting within the offshore
1007 western Gulf of Corinth, Greece: implications for models of continental rift deformation.
1008 *Geology,* 33, 241–244.
1009 MITCHUM, R.M., VAIL, P.R. & THOMPSON, S. (1977) Seismic stratigraphy and global changes
1010 of sea level, Part 2: The depositional sequence as a basic unit for stratigraphic analysis. In:
1011 Seismic Stratigraphy – Applications to Hydrocarbon Exploration (Ed. by C.E. Payton), *AAPG*
1012 *Mem.,* 26, 53-62.
1013 MORETTI, I., LYKOUSIS, V., SAKELLARIOU, D., REYNAUD, J.Y., BENZIANE, B. & PRINZHOFFER,
1014 A. (2004) Sedimentation and subsidence rate in the Gulf of Corinth: what we learn from the
1015 Marion Dufresne's long-piston coring. *C.R. Geosci.,* 336, 291-299.
1016 MORTIMER, E., GUPTA, S. & COWIE, P. (2005) Clinoform nucleation and growth in coarse-
1017 grained deltas, Loreto basin, Baja California Sur, Mexico: a response to episodic accelerations
1018 in fault displacement. *Basin Research*, 17, 337-359.
1019 NEAL, J. & ABREU, V. (2009) Sequence stratigraphy hierarchy and the accommodation
1020 succession method. *Geology*, 37, 779-782.
1021 NIXON, C.W., MCNEILL, L.C., BULL, J.M., BELL, R.E., GAWTHORPE, R.L., HENSTOCK, T.J.,
1022 CHRISTODOULOU, D., FORD, M., TAYLOR, B., SAKELLARIOU, D., FERENTINOS, G.,
1023 PAPATHEODOROU, G., LEEDER, M.R., COLLIER, R.E.L., GOODLIFFE, A.M., SACHPAZI, M. &
1024 KRANIS, H. (2016) Rapid spatiotemporal variations in rift structure during development of the
1025 Corinth Rift, central Greece. *Tectonics,* 35, 1225-1248.
1026 ORI, G.G., ROVERI, M. & NICHOLS, G. (1991) Architectural patterns in large-scale Gilbert-type
1027 delta complexes, Pleistocene, Gulf of Corinth, Greece. In: The Three-Dimensional Facies

1028 Architecture of Terrigenous Clastic Sediments and Its Implications for Hydrocarbon Discovery
1029 and Recovery Miall, (Ed. by A.D. Miall & N. Tyler), *Concepts in Sedimentology and*
1030 *Paleontology, 3. Society for Sedimentary Geology (SEPM),* 207-216.
1031 PERISSORATIS, C., PIPER, D.J. & LYKOUSIS, V. (2000) Alternating marine and lacustrine
1032 sedimentation during the late Quaternary in the Gulf of Corinth rift basin, central Greece:
1033 *Marine Geology*, 167, 391–411.
1034 RITCHIE, B.D., HARDY, S. & GAWTHORPE, R.L. (1999) Three dimensional numerical modeling
1035 of coarse-grained clastic deposition in sedimentary basins. *Journal of Geophysical Research*,
1036 104, 17759-17780.
1037 ROHAIS, S., ESCHARD, R., FORD, M., GUILLOCHEAU, F. AND MORETTI, I. (2007) Stratigraphic
1038 architecture of the Plio-Pleistocene infill of the Corinth Rift: implications for its structural
1039 evolution. *Tectonophysics,* 440, 5-28.
1040 SCHOLZ, C. (2010) Large earthquake triggering, clustering, and the synchronization of faults.
1041 *Bull. Seismol. Soc. Am.,* 100, 901–909.
1042 SCHWARTZ, D. P. & COPPERSMITH, K. J. (1984) Fault behaviour and characteristic earthquakes
1043 - examples from the Wasatch and San Andreas fault zones. *J. Geophys. Res.,* 89, 5681-5698.
1044 SOTER, S. & KATSONOPOULOU, D. (1998) The search for ancient Helike, 1988–1995:
1045 geological, sonar and bore hole studies. In: *Ancient Helike and Aigalieia* (ed. by
1046 Katsonopoulou, D., Soter, S. & Scilardi, D.). The Helike Society, Aigion, pp. 67-116.STEVENSON,
1047 C.J., JACKSON, C.A.L., HODGSON, D.M., HUBBARD, S.M., EGGENHUISEN, J.T. (2015) Deep-
1048 water sediment bypass. *Journal of Sedimentary Research*, 85, 1058-1081.
1049 SUC, J-P. & POPESCU, S-M. (2005) Pollen records and climatic cycles in the North
1050 Mediterranean region since 2.7 Ma. *Geological Society, London, Special Publications,* 247,
1051 147-158.
1052 TORFSTEIN, A., GOLDSTEIN, S.L., STEIN, M. & ENZEL, Y. (2013) Impacts of abrupt climate
1053 changes in the Levant from Last Glacial Dead Sea levels. *Quaternary Science Reviews*, 69, 1-7.
1054 WDOWINSKI, S., O'CONNELL, R.J. & ENGLAND, P. (1989). A continuum model of continental
1055 deformation above subduction zones' application to the Andes and the Aegean. *Journal of*
1056 *Geophysical Research*, 94, 10331-10346.
1057
1058
1059

List of Figures

(2010). Middle-upper units, Units 7-11 are the focus at Selinous and lower-middle units, Units 2-7 are the focus at Kerinitis. Insets show position (black box) in the context of each fan delta on wider 3D outcrop models. Locations of sections are shown in Fig. 1.

Figure 5. Sedimentological details of Facies Associations 1-3 – fluvial topsets, shallow water topsets and foresets. A) FA 1: log and field photograph of FA 1b (delta plain fluvial topset) highlighting presence of palaeosol horizons, and field photograph of FA 1a (fluvial channel fill). B) FA 2: sketch and field photograph of FA 2a (beach barrier) and field photograph of FA 2b (lower shoreface). Note m-scale asymptotic hummocky cross-stratification in FA 2b. Sketch of the outcrop section revealing FA 2a is provided to highlight key features – m-scale, bi-directional cross-beds, texturally mature clasts and normally graded cycles (facies Co5). Facies Co5 is subdivided here to show fining upwards cycles (1-3); 1 = poorly-sorted, matrix-supported, rounded gravel-pebble conglomerate; 2 = open-framework rounded pebbles; 3 = poorly-sorted gravel. 3) FA 3: field photographs of 10 m-scale and 100 m-scale foresets at Selinous and Kerinitis, and sketch log of foresets at Unit 11, Selinous Location S3.

Figure 6. A) Field photographs of FAs 4a and 4b. B) Log of FA4b from the fine interval between Units 10 and 11 at Selinous Location S3. C) Log of FA4c from the fine interval between Units 5 and 6 at Kerinitis Location K2. D) Field photographs of FA4c – note symmetrical ripples, indicating shallow water depth.

Figure 7. Geometric position of shallow water bottomsets (FA4c). A) Diagram shows the position of two hypothetical delta units X and Y to show the juxtaposition of underlying topsets of Y and overlying bottomsets of X in shallow water. The bottomsets of X are in a water depth above storm wave base and therefore present shallow water facies even though they are geometric bottomsets. B) Sketch of the modern Selinous fan delta (X), prograding over the Late Pleistocene Selinous fan delta (Y) as an example of the juxtaposition shown in A (position shown in Fig. 1). Bathymetry data from Cotterill et al. (2002) and McNeill et al. (2005).

Figure 8. Sketch and field photographs to present an erosional surface apparent at Selinous Location S2 between Units 8 and 9, interpreted to be a sequence boundary. Photographs shown from KSS2 between Units 1 and 2 of a non-erosive surface at Kerinitis as comparison. Geologist for scale is 1.75 m. Numbers indicated in blue represent Facies Association codes.

Figure 9. Summary diagram of architectural stacking at both fan deltas in their respective positions along the P-M Fault. Trajectory analyses of topset-foreset breakpoint of both fan deltas are shown alongside the cross-sections. Topset-foreset breakpoints are shown by black filled circles and trajectory paths are shown by black lines. Study Locations S1-3 and K1-3 are indicated. Unit thicknesses on trajectory analysis diagrams are normalised to emphasise the relative patterns in the trajectory styles. The trajectory of Unit 4 is less certain (question marks). Solid lines show observable trajectories in the transition zone and dashed lines show our interpretation of retrogradation back to the fault and/or correlative surfaces to downdip maximum flooding surfaces. Kerinitis cross-section from Gawthorpe et al. (2017a) after Backert et al. (2010).

Figure 10. Input parameters for numerical model Syn-Strat, derived from field observations, and example outputs. A) Relative base level curve inputs and output: A1) 1D input curves representing subsidence and lake level in time and space; A2) the subdivision of a relative base level curve that is applied to the 3D surfaces; A3) resultant surface showing 3D relative base level through time, along the length of the fault. B) Sedimentation inputs incorporated to produce an accommodation surface: B1) 1D inputs of sedimentation in time and space B2) schematic diagram with red line to indicate position of the plots relative to the fault, i.e. a position in the immediate hangingwall of the fault; B3) resultant 3D accommodation surface. Positions of Kerinitis and Selinous are shown by K and S labels, respectively. Sequence boundaries are positioned between yellow and purple sections and are apparent at the fault tips, but absent towards the fault centre in both A3 and B3. Note reduced accommodation at fan delta locations in B3 due to sediment-filling. Amplitude of lake level change is varied in the sensitivity tests (pale yellow). EFT = East Fault Tip; WFT = West Fault Tip.

Figure 11. Results from numerical modelling sensitivity tests with Syn-Strat. The amplitude of lake level (A) is varied from 5 m to 30 m at 5 m intervals. 3D accommodation surface is shown as example (B). Flattened accommodation surfaces are presented for each test with stages of base level curve presented to allow visualisation of stratigraphic surface extent (CI-CVI). Sequence boundaries (SBs) are between yellow and purple sections. Positions of Kerinitis and Selinous are shown by K and S labels, respectively. Approximate outcrop section positions are indicated by dashed lines. The 5 m amplitude test (CI) reveals sequence boundary absence at both outcrop section positions, and the 20-30 m (CIV-CVI) amplitude tests reveal the presence

of sequence boundaries at both outcrop section positions – not comparable to field observations. The 10 m and 15 m amplitude tests (CII and CIII, highlighted in green) reveal absence of sequence boundaries at the outcrop section position at Kerinitis and presence of sequence boundaries at the outcrop section position at Selinous – most comparable to field observations – refining the amplitude of lake level fluctuations during the Early-Middle Pleistocene to 10-15 m.

Figure 12. Along-strike graphical cross-section to show unit thickness decay extrapolation towards the western fault tip. This is to derive a hypothetical unit thickness at the fault tip, where subsidence is zero and any remaining thickness may have accumulated in space derived from base level change, thus providing an independent derivation of the amplitude of base level change through the Early-Middle Pleistocene in Lake Corinth (12 m), in support of our modelling results (10-15 m). The semi-circular lines are presented to show the extent of the deltas along the fault and to highlight the greater thickness of Kerinitis than Selinous.

List of tables

Table 1. Summary of facies associations with geometric position and depositional environment interpretations.

Table 2. Quantitative field observations and control parameter derivations, with assigned uncertainty values (1-5). 1 = low uncertainty; 5 = high uncertainty.

APPENDIX

Table A. Summary of sedimentary facies identified across Selinous and Kerinitis deltas with code, description and indication of corresponding facies codes from Backert et al. (2010) from Kerinitis. Facies abbreviations: Co, conglomerates; Sa, sandstones, Fi, siltstones and mudstones.

Figure 1

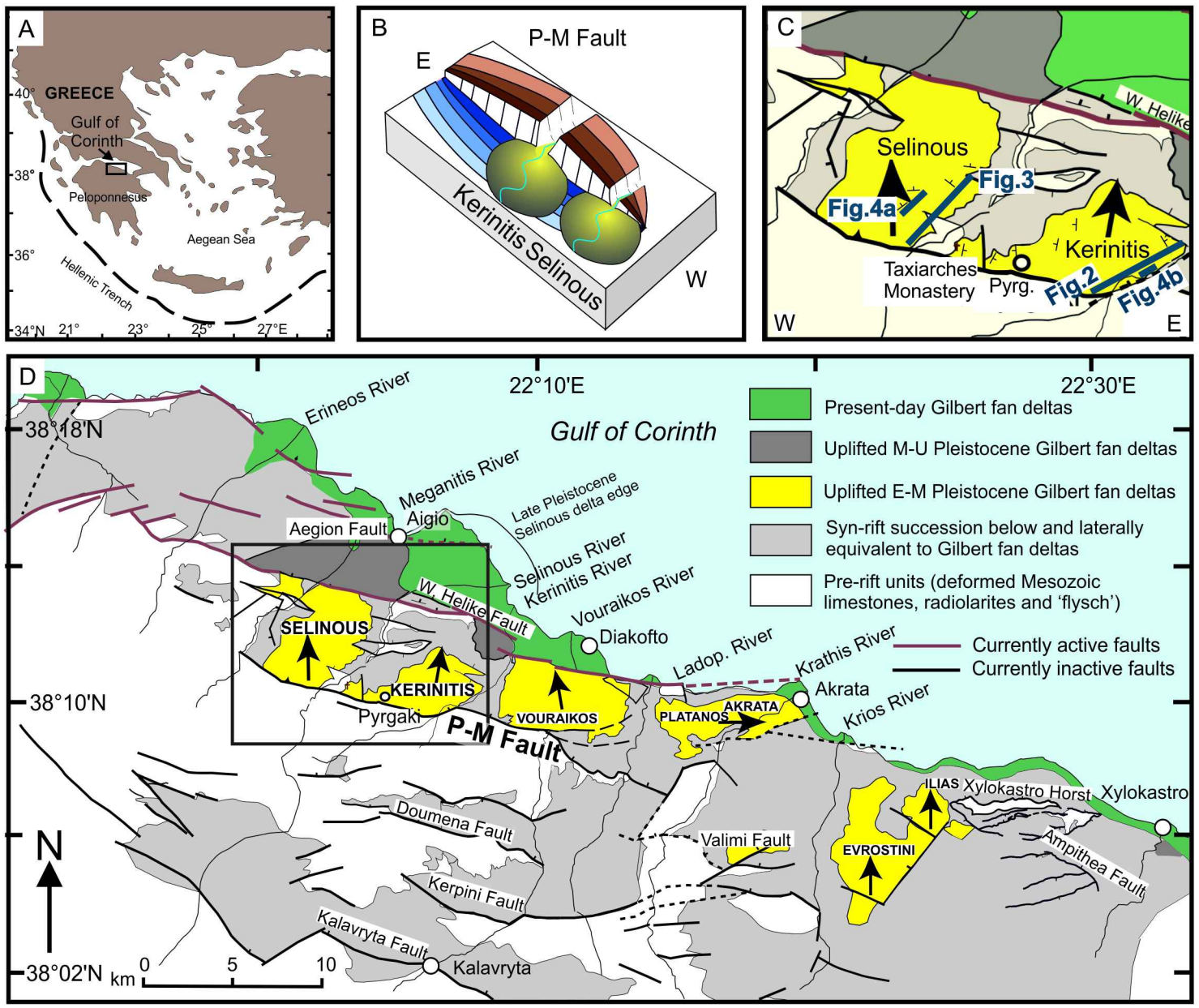
A
GREECE
Gulf of Corinth
Peloponnesus
Aegean Sea
Hellenic Trench
40°
38°
36°
34°N
21°
23°
25°
27°E
B
P-M Fault
E
W
Kerinitis Selinous
C
W. Helike
Selinous
Fig.3
Fig.4a
Kerinitis
Taxiarches Monastery
Pyrg.
Fig.2
Fig.4b
W
E
D
22°10'E
22°30'E
38°18'N
38°10'N
38°02'N
Erineos River
Gulf of Corinth
Meganitis River
Late Pleistocene Selinous delta edge
Aegion Fault
Aigio
Selinous River
Kerinitis River
Vouraikos River
W. Helike Fault
SELINOUS
KERINITIS
Pyrgaki
VOURAIKOS
Diakofto
Ladop. River
Krathis River
Akrata
Krios River
AKRATA
PLATANOS
P-M Fault
ILIAS
Xylokastro Horst
Xylokastro
Doumena Fault
Valimi Fault
EVROSTINI
Ampithea Fault
Kerpini Fault
Kalavryta Fault
Kalavryta
N
0
5
10
km
Present-day Gilbert fan deltas
Uplifted M-U Pleistocene Gilbert fan deltas
Uplifted E-M Pleistocene Gilbert fan deltas
Syn-rift succession below and laterally equivalent to Gilbert fan deltas
Pre-rift units (deformed Mesozoic limestones, radiolarites and 'flysch')
Currently active faults
Currently inactive faults

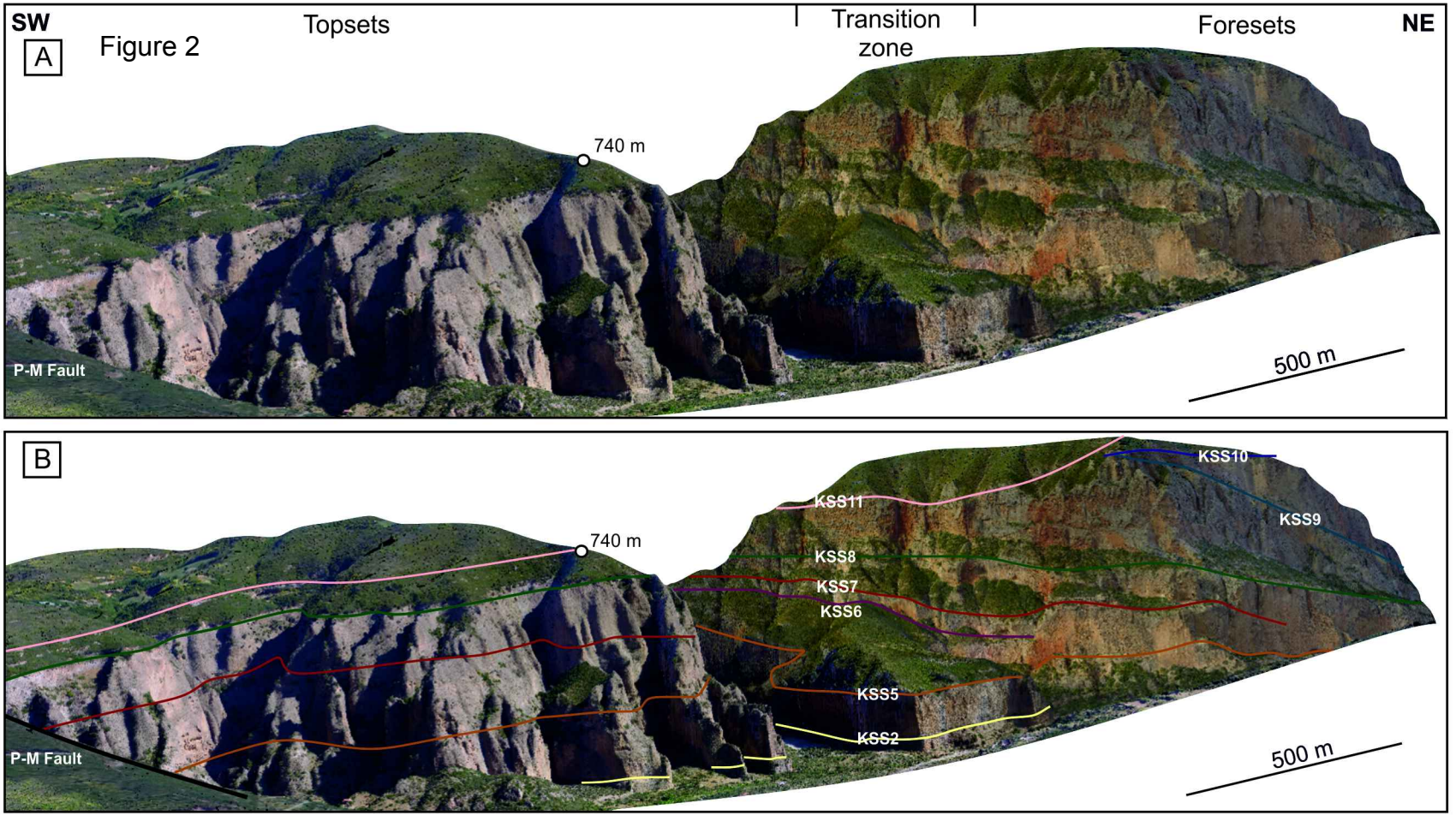
SW
A
Figure 2
Topsets
Transition zone
Foresets
NE
740 m
P-M Fault
500 m
B
KSS10
KSS11
KSS9
740 m
KSS8
KSS7
KSS6
KSS5
KSS2
P-M Fault
500 m

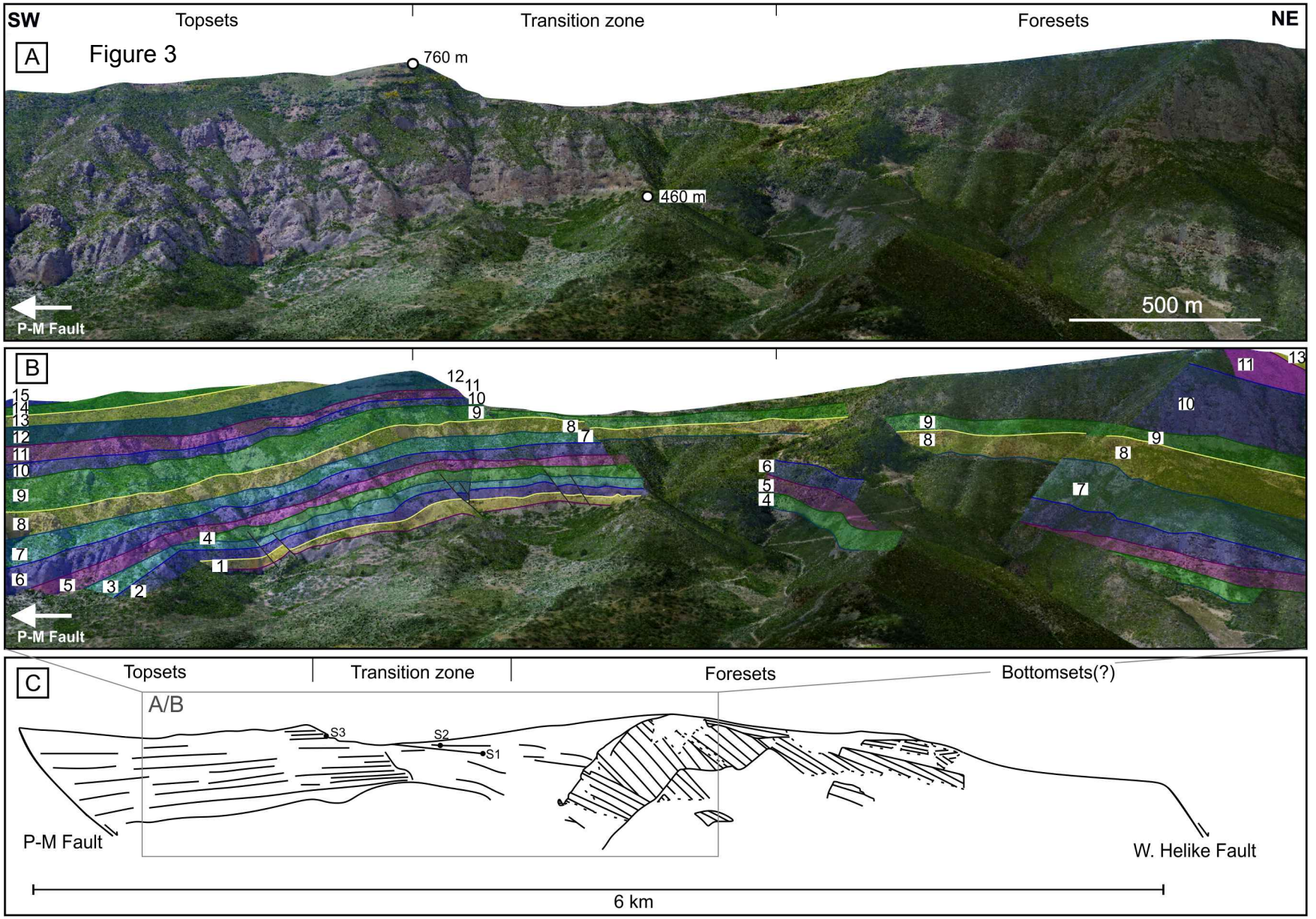
SW
Topsets
Transition zone
Foresets
NE
A
Figure 3
760 m
460 m
500 m
P-M Fault
B
P-M Fault
C
Topsets
Transition zone
Foresets
Bottomsets(?)
A/B
S3
S2
S1
P-M Fault
W. Helike Fault
6 km

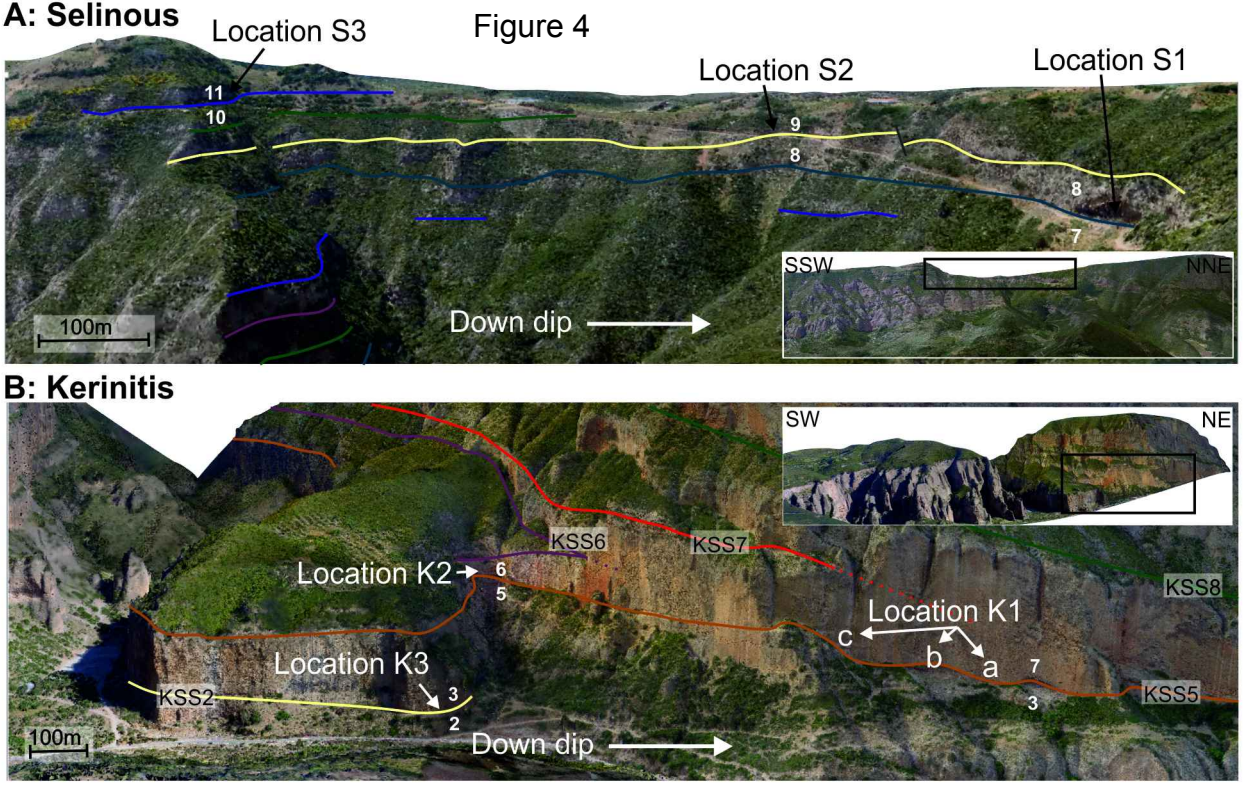
A: Selinous
Location S3
Figure 4
Location S2
Location S1
11
10
9
8
8
7
SSW
NNE
100m
Down dip
B: Kerinitis
SW
NE
KSS6
KSS7
KSS8
Location K2
6
5
Location K1
c
b
a
7
3
Location K3
KSS2
3
2
KSS5
100m
Down dip

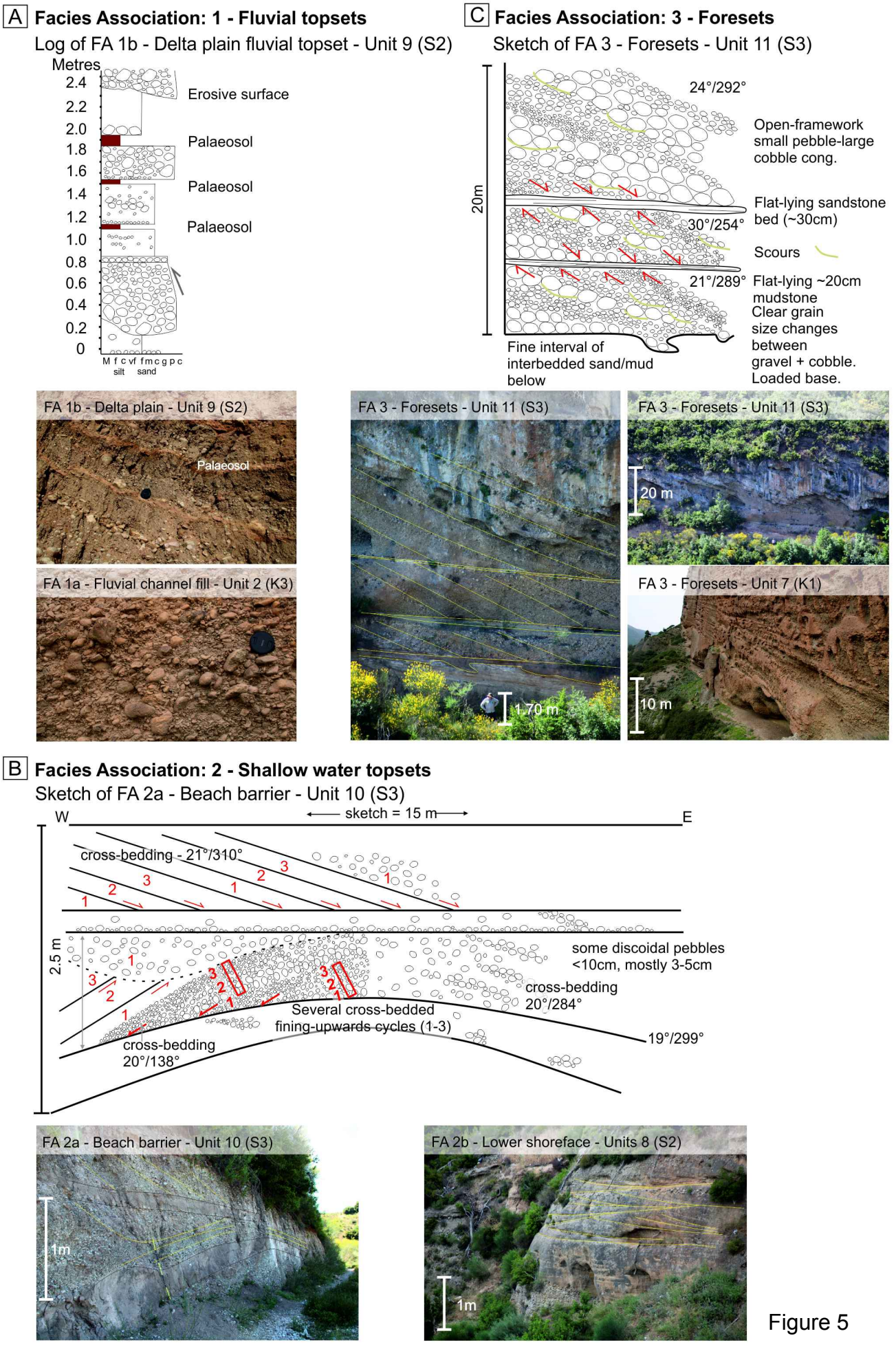
A Facies Association: 1 - Fluvial topsets
Log of FA 1b - Delta plain fluvial topset - Unit 9 (S2)
Metres
2.4
2.2
2.0
1.8
1.6
1.4
1.2
1.0
0.8
0.6
0.4
0.2
0
M f c vf f m c g p c
silt
sand
Erosive surface
Palaeosol
Palaeosol
Palaeosol
C Facies Association: 3 - Foresets
Sketch of FA 3 - Foresets - Unit 11 (S3)
20m
24°/292°
30°/254°
21°/289°
Open-framework small pebble-large cobble cong.
Flat-lying sandstone bed (~30cm)
Scours
Flat-lying ~20cm mudstone
Clear grain size changes between gravel + cobble. Loaded base.
Fine interval of interbedded sand/mud below
FA 1b - Delta plain - Unit 9 (S2)
Palaeosol
FA 1a - Fluvial channel fill - Unit 2 (K3)
FA 3 - Foresets - Unit 11 (S3)
1.70 m
FA 3 - Foresets - Unit 11 (S3)
20 m
FA 3 - Foresets - Unit 7 (K1)
10 m
B Facies Association: 2 - Shallow water topsets
Sketch of FA 2a - Beach barrier - Unit 10 (S3)
W
sketch = 15 m
E
cross-bedding - 21°/310°
2.5 m
some discoidal pebbles <10cm, mostly 3-5cm
cross-bedding 20°/284°
Several cross-bedded fining-upwards cycles (1-3)
19°/299°
cross-bedding 20°/138°
FA 2a - Beach barrier - Unit 10 (S3)
1m
FA 2b - Lower shoreface - Units 8 (S2)
1m

Figure 5

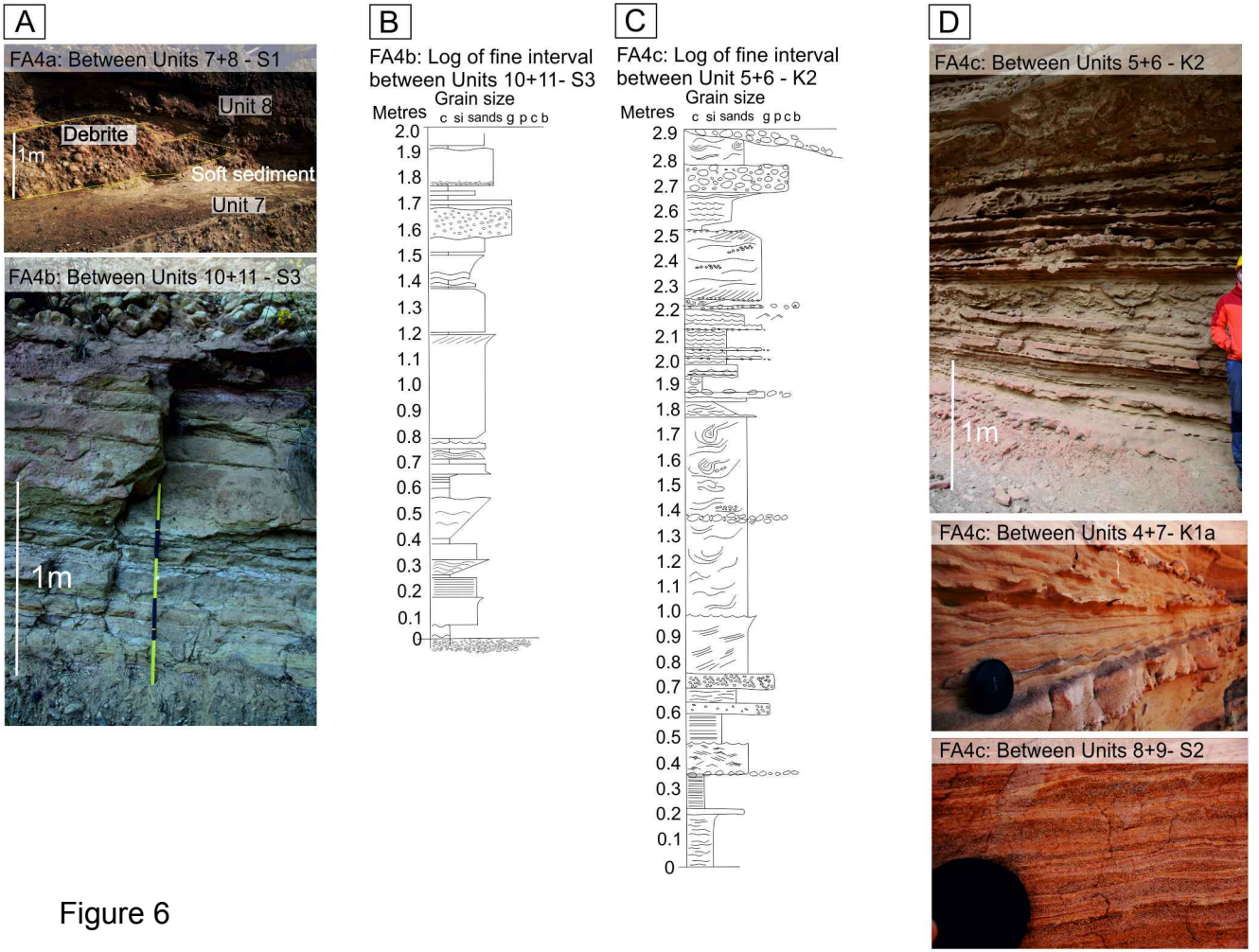
A
FA4a: Between Units 7+8 - S1
Unit 8
Debrite
1m
Soft sediment
Unit 7
FA4b: Between Units 10+11 - S3
1m
B
FA4b: Log of fine interval between Units 10+11- S3
Grain size
Metres
c si sands g p c b
2.0
1.9
1.8
1.7
1.6
1.5
1.4
1.3
1.2
1.1
1.0
0.9
0.8
0.7
0.6
0.5
0.4
0.3
0.2
0.1
0
C
FA4c: Log of fine interval between Unit 5+6 - K2
Grain size
Metres
c si sands g p c b
2.9
2.8
2.7
2.6
2.5
2.4
2.3
2.2
2.1
2.0
1.9
1.8
1.7
1.6
1.5
1.4
1.3
1.2
1.1
1.0
0.9
0.8
0.7
0.6
0.5
0.4
0.3
0.2
0.1
0
D
FA4c: Between Units 5+6 - K2
1m
FA4c: Between Units 4+7- K1a
FA4c: Between Units 8+9- S2

Figure 6

Figure 7

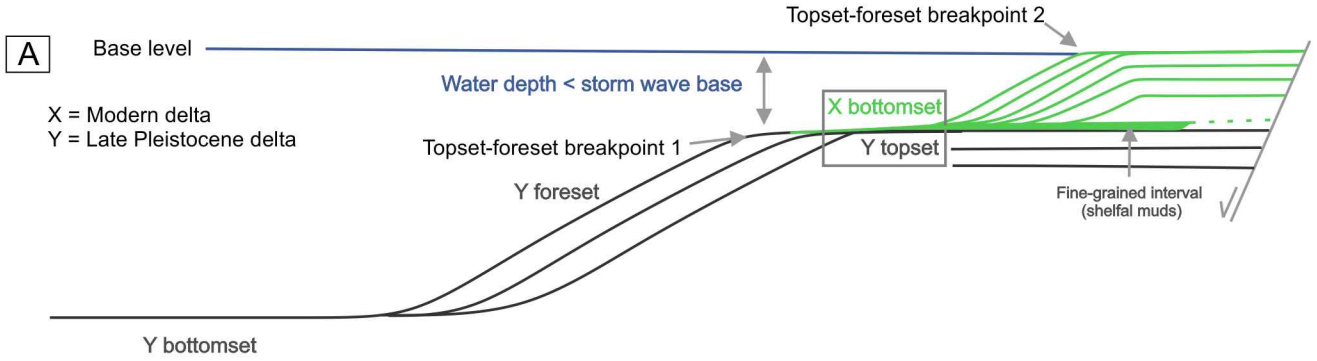
A
Base level
Topset-foreset breakpoint 2
Water depth < storm wave base
X = Modern delta
Y = Late Pleistocene delta
X bottomset
Topset-foreset breakpoint 1
Y topset
Y foreset
Fine-grained interval
(shelfal muds)
Y bottomset

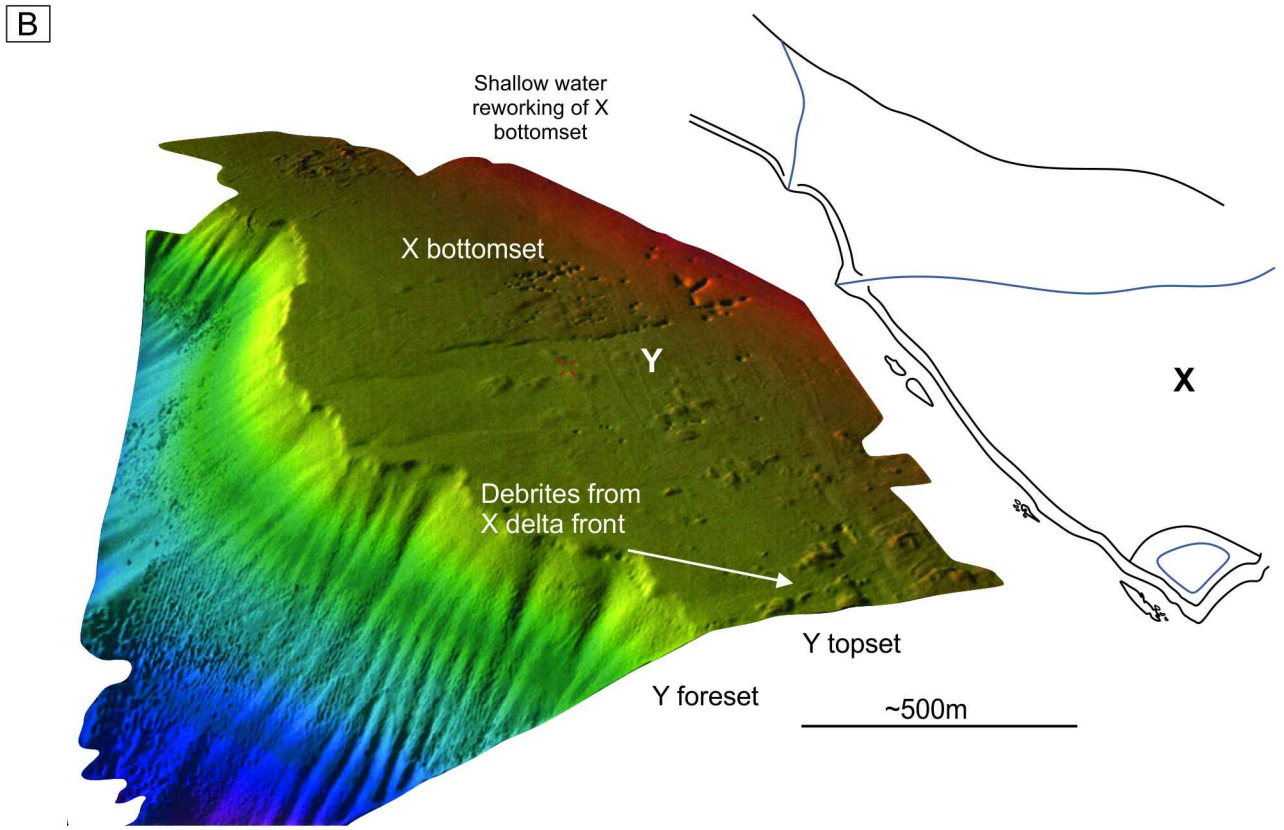
B
Shallow water
reworking of X
bottomset
X bottomset
Y
X
Debrites from
X delta front
Y topset
Y foreset
~500m

Selinous surface character

Location S2

Several m of erosion at surface. Interpreted as a sequence boundary.

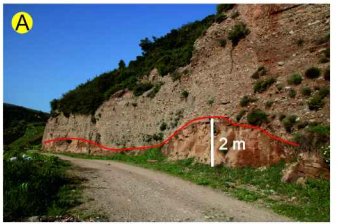

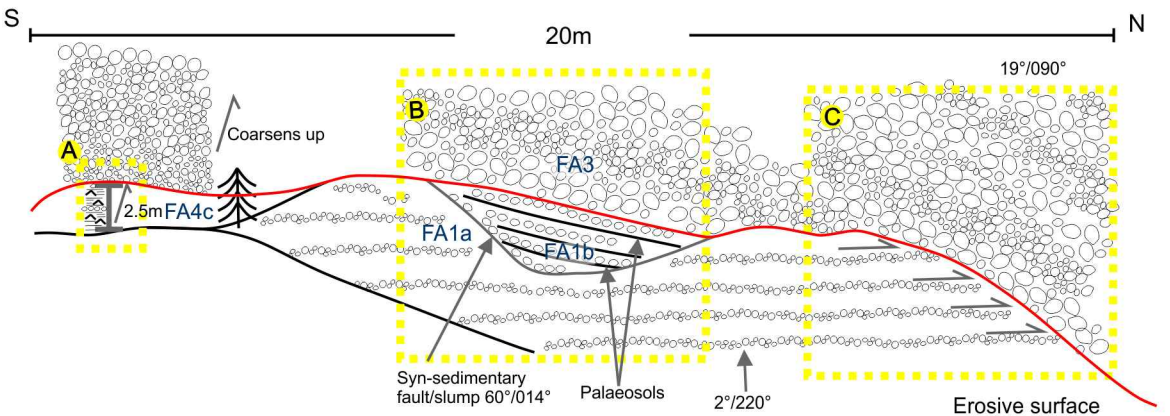

Kerinitis surface character

Location K3

Minor erosion at surface. Not a sequence boundary.

Figure 8

Figure 9

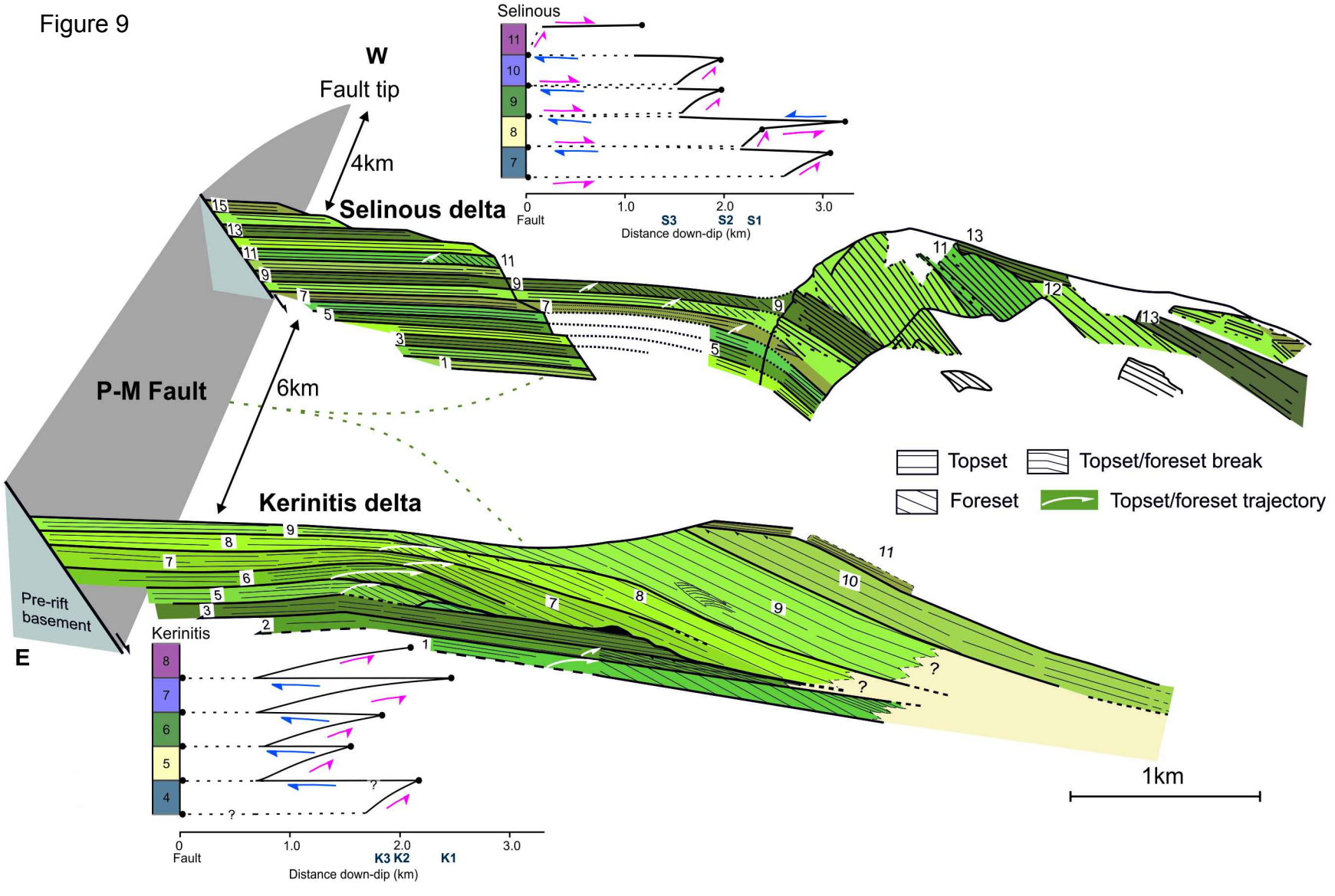
W
Fault tip
4km
Selinous
Selinous delta
P-M Fault
6km
Kerinitis delta
Pre-rift basement
E
Kerinitis
Fault
S3 S2 S1
K3 K2 K1
Distance down-dip (km)
Topset
Topset/foreset break
Foreset
Topset/foreset trajectory
1km

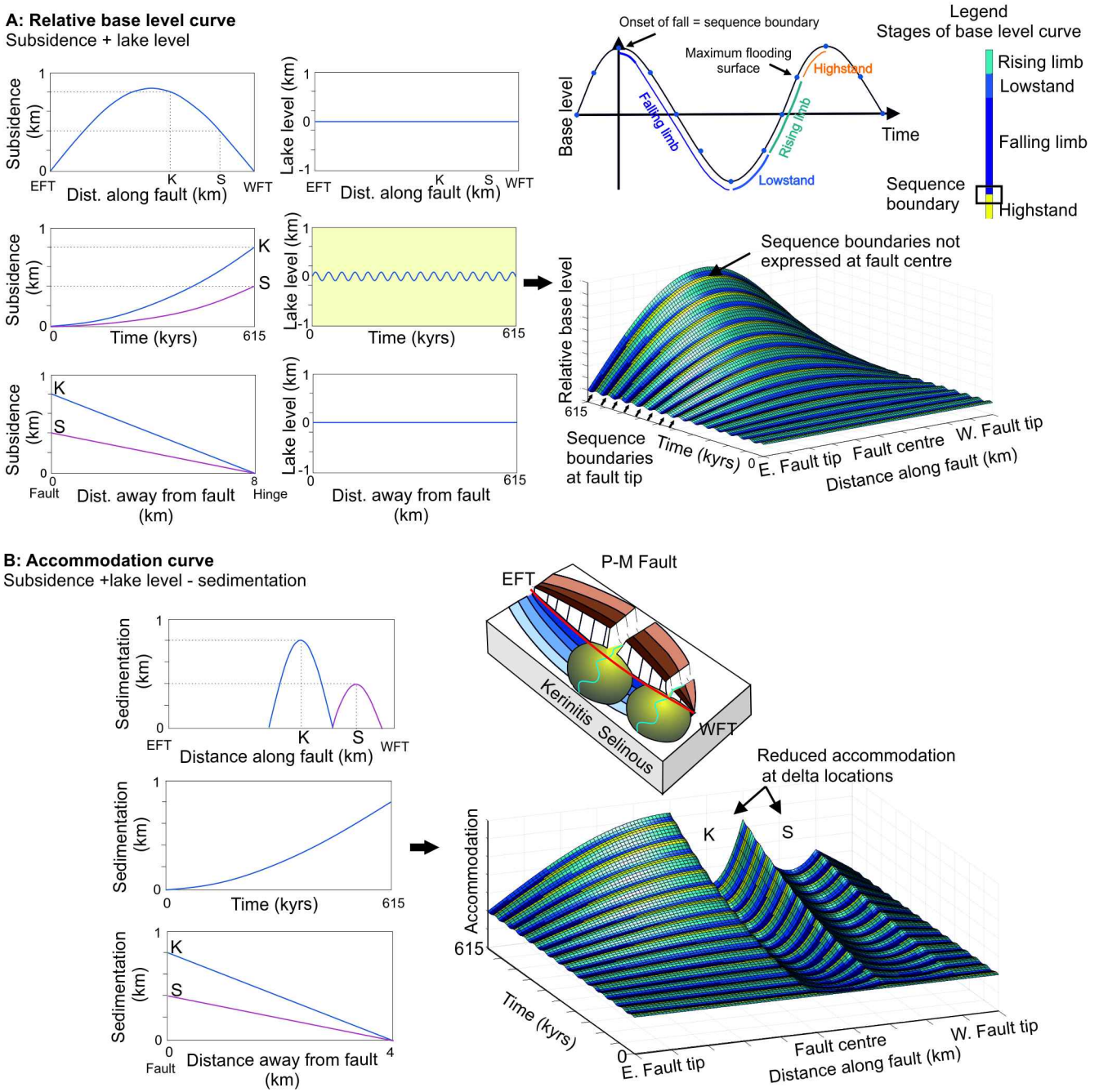

Parameter to vary

Figure 10

Figure 11

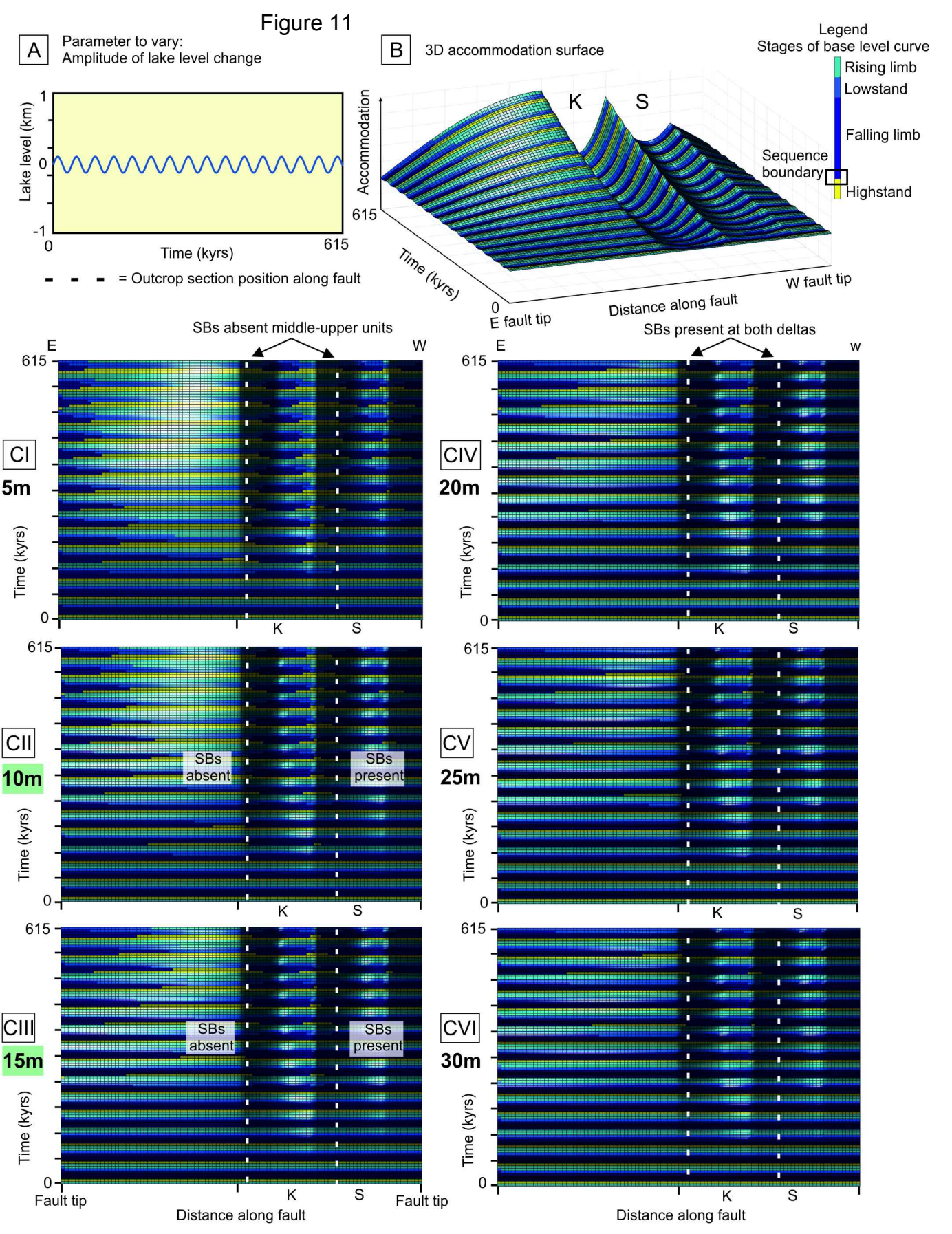
A
Parameter to vary:
Amplitude of lake level change
Lake level (km)
1
0
-1
0
Time (kyrs)
615
= Outcrop section position along fault
B
3D accommodation surface
Accommodation
615
Time (kyrs)
0
E fault tip
Distance along fault
W fault tip
K
S
Legend
Stages of base level curve
Rising limb
Lowstand
Falling limb
Sequence boundary
Highstand
SBs absent middle-upper units
SBs present at both deltas
E
W
w
615
0
Time (kyrs)
CI
5m
CII
10m
CIII
15m
CIV
20m
CV
25m
CVI
30m
K
S
SBs absent
SBs present
Fault tip
Distance along fault

Figure 12

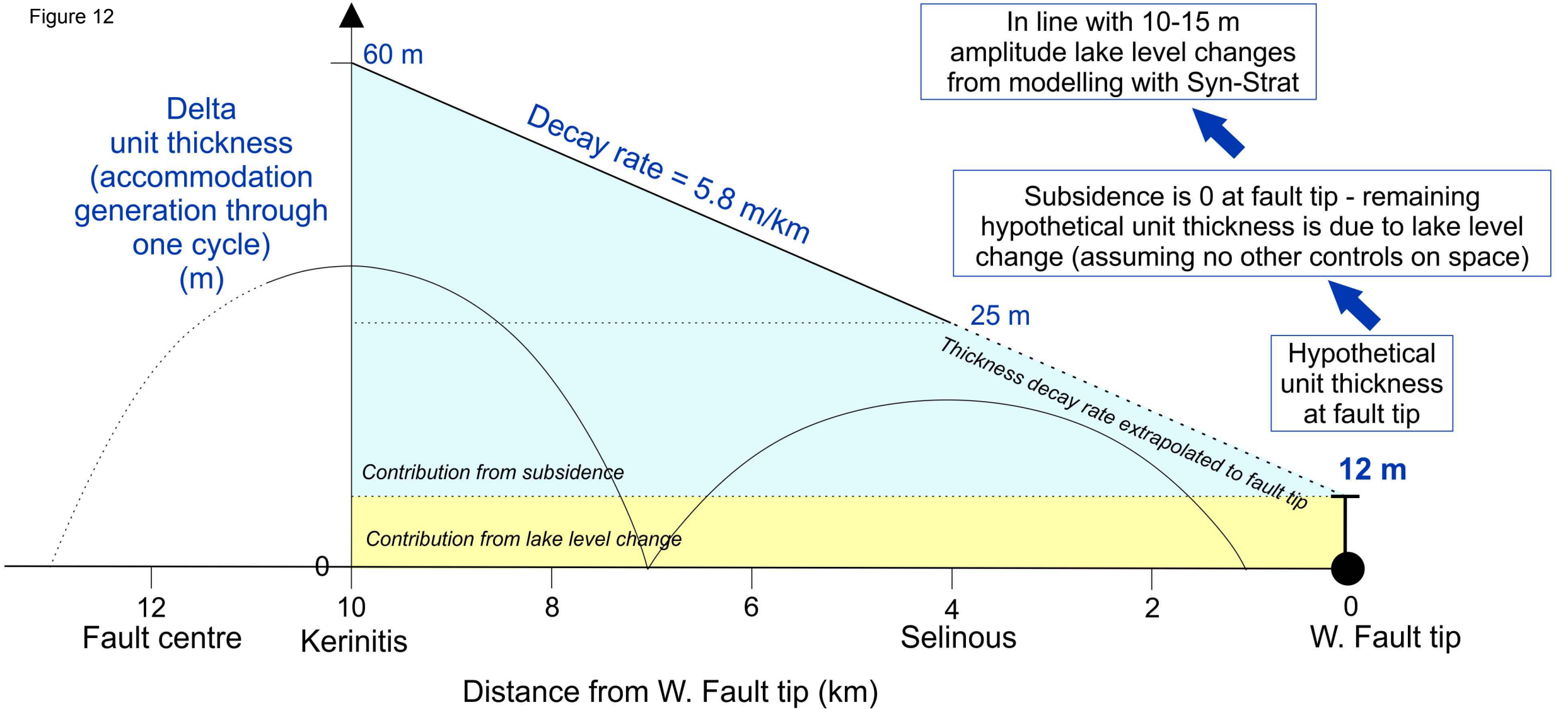
In line with 10-15 m amplitude lake level changes from modelling with Syn-Strat
Subsidence is 0 at fault tip - remaining hypothetical unit thickness is due to lake level change (assuming no other controls on space)
Hypothetical unit thickness at fault tip
Delta unit thickness (accommodation generation through one cycle) (m)
60 m
Decay rate = 5.8 m/km
25 m
Thickness decay rate extrapolated to fault tip
12 m
Contribution from subsidence
Contribution from lake level change
0
12
Fault centre
10
Kerinitis
8
6
4
Selinous
2
0
W. Fault tip
Distance from W. Fault tip (km)

FA code	Constituent facies	FA interpretation	Sub-association
1a	Co1, Co2	Fluvial topset	Channel fill
1b	Co1, Sa2, Sa6, Fi3		Delta plain
2a	Co4, Co5	Shallow water topset	Beach barrier
2b	Co5		Lower shoreface
3	Co3, Co4, Sa4	Foreset	
4a	Sa1, Sa3, Fi1, Fi2, Fi4	Bottomset	Distal
4b	Sa1, Sa2, Sa4, Sa5, Fi1-3, Fi5, Fi6		Intermediate
4c	Co6, Sa1-6, Fi1, Fi2		Proximal

	Parameter	Selinous	Kerinitis	Uncertainty value (1-5)
Observations	Number of units	15	11	1
	Total thickness of deltas	~400 m	>800 m	1
	Thickness of units	25 m	60 m	1
	Distance between the two deltas	6 km		1
	Unit thickness decay rate along fault	5.8 m/km		1
Interpretations	Total subsidence	~400 m	>800 m	1
	Climate change periodicity	~41 kyrs		1
	Lake level change periodicity	~41 kyrs		2
	Delta build time	615 kyrs	>451 kyrs	2
	Subsidence rate	0.65 m/kyrs	>1.77 m/kyrs	2
	Magnitude of lake level rise through each climatic cycle	<25 m 10-15 m*[1] 12 m*[2]		4 2*[1] 2*[2]
	Average sedimentation rate	0.65 m/kyrs	>1.77 m/kyrs	2
	Sedimentation model through time	Variable		4

*[1] Values refined from numerical modelling exercise with Syn-Strat

*[2] Values refined using independent thickness extrapolation method

Facies code	Facies description	Process interpretation	Backert et al. (2010) scheme code
Co1: Matrix-supported conglomerate	Poorly-sorted, matrix-supported (sand-gravel), gravel-cobble grade conglomerate. Sub-rounded to sub-angular clasts <15 cm. Some cases of normal grading to fine sand. Cm- to dm-thick beds.	High energy bedload transport	G2: Matrix-supported conglomerate
Co2: Stratified conglomerate	Poorly-sorted, variable matrix- and clast-support (sand-gravel), pebble-cobble grade conglomerate, sub-horizontal bedding. Cm- to dm-thick beds.	Bedload transport/longitudinal bedforms	G1c: Crudely stratified conglomerate
Co3: Dipping conglomerate	Steeply dipping (~25°), poorly-sorted, clast-supported gravel-boulder conglomerate. Mostly sub-rounded, large pebble and cobble clasts (<15 cm diameter), occasional small boulders (<25 cm). Matrix of coarse sand-gravel. In some cases locally imbricated. <1m thick open framework lenses. Cuts and scours. >10 m-thick beds.	Gilbert-type delta foresets, characterised by erosive sediment gravity flows on steep slopes	G1b: Steeply dipping conglomerate
Co4: Clast-supported conglomerate	Well to poorly-sorted, clast-supported, pebbly conglomerate with occasional cobbles. Mainly sub-rounded to sub-angular clasts (<10 cm). Inverse grading. Some beds pinch out laterally. Cm-dm thick beds.	Granular flow	G1a: Well-to poorly-sorted structureless conglomerate
Co5: Cross-bedded conglomerate	Well-sorted, matrix- and clast-supported parts (some open-framework), gravel-cobble conglomerates. Clasts are mainly rounded-discoidal (<16 cm). Dm- to m-scale cross-beds with 21-24° dip, locally with an asymptotic geometry. Some beds pinch out laterally. Inverse and normal grading within beds and gradational contacts.	Dune migration by bedload transport and wave and storm reworking	G1e: Cross-stratified conglomerate
Co6: Interbedded conglomerate-gravelly sand	Mostly poorly-sorted, matrix-supported interbedded pebble-cobble grade conglomerate and gravelly coarse sand. Sand is generally laminated with gravel and with dispersed pebbles. Some cobble beds are open-framework and well-sorted or poorly-sorted and clast-supported. Beds <20 cm thick.	Variable energy regime sediment gravity flows - avalanche grain flows and high density turbidity currents	
Sa1: Graded sandstone	Well-sorted, inverse or normal grading, very fine-very coarse sandstone. Mainly massive, but in some cases with some parallel laminations at the base or faint cross-beds near the top. Cm- to dm-thick beds.	Turbidity current – Bouma TA-C	S4: Inversely or normal graded sandstone
Sa2: Massive sandstone	Poorly-sorted, massive fine-medium sandstone with cm-scale gravel lag at bases. Some cases evidence of weak normal grading. Dm-thick beds.	Medium energy flow regime, bedload transport	S1: Structureless sandstone
Sa3: Interbedded sand and gravel lenses with shell clusters	Interbedded fine sand and gravel lenses (<5 cm thick and <50 cm length), pinching out over 15-150cm. Occasional sub-rounded pebble clasts. Some gravel lenses fine laterally into fine-medium sand. Broken shell fragments, often in clusters within red-coloured gravelly-coarse sand matrix. Dm-thick beds.	Storm current reworking shallow marine sediment and transporting downdip	

Sa4: Planar- and wavy-laminated sandstone	Flat-lying, planar- or wavy-laminated very fine-fine sandstone. Sometimes inversely graded. Cm- to dm-thick beds.	Upper stage plane beds with variable flow conditions	S2: Laminated sandstone
Sa5: Cross-bedded sandstone	Low-angle cross-bedded very fine-medium sand. Medium sand grade lenses (<2 cm long and ~0.5 cm thick). Symmetrical and/or asymmetrical ripples with silt drapes (<0.5 cm). Cm- to dm-thick beds.	Wave or current ripple and dune migration with periods of intermittent quiescence	S3: Cross-bedded sandstone
Sa6: Gravelly sandstone	Poorly-sorted, gravelly coarse sand, some gravelly laminations and small floating pebbles. Sometimes with erosive base. Cm- to dm-thick beds.	Medium energy bedload transport or high density turbidity current	S1: Structureless sandstone
Fi1: Wavy-laminated siltstone	Wavy-laminated, ripple cross-bedded, fine calcareous siltstone with scours and soft sediment deformation. Normal or inverse grading. Cm-width, 10cm-length sand- and mud-filled *Planolites* burrows. Cm-thick beds.	Occasional turbidity current events – Bouma TD-E – with periods of quiescence for colonisation. Loading from dense conglomerate above	F2: Laminated siltstone
Fi2: Planar-laminated siltstone	Planar-laminated siltstone (cm- to dm-thick beds). Some variations in colour from red - cream – orange.	Suspension fall-out and intermittent dilute turbidity current	F2: Laminated siltstone
Fi3: Red-coloured sandy siltstone	Varying thickness (cm-scale) red-coloured sandy silt.	Palaeosol	F3b: Variegated siltstone
Fi4: Organic-rich, structureless mudstone	Structureless claystone, dark colour - organic rich. Cm-thick beds.	Suspension fall-out with anoxic conditions	
Fi5: Structureless mudstone	Structureless calcareous mudstone. Cream or red coloured. Cm- to dm-thick beds.	Suspension fall-out	F4a: Claystone
Fi6: Interbedded sandstone-mudstone	Interbedded wavy very fine sandstone and white or pink coloured mudstone. Cm-thick beds.	Suspension fall-out and intermittent dilute turbidity current	F3a: Interbedded siltstone